ELECTRICAL AND OPTICAL INVESTIGATIONS
OF BETA-GALLIUM OXIDE

Thesis by
Michael Paul Anthony

In Partial Fulfillment of the Requirements
For the Degree of
Doctor of Philosophy

California Institute of Technology
Pasadena, California
1972
(Submitted December 17, 1971)

To my wife, Jocelyn

ACKNOWLEDGEMENT

My years as a graduate student at Caltech have been a period of great personal growth for me; I wish to express my enormous gratitude to my advisor, Professor Carver Mead, whose perseverance, encouragement, criticism and concern were literally invaluable.

Thanks are due especially to Ingrid Vierheilig, who provided help and encouragement as well as most of the typing of this thesis, as well as to Carol Norris and the other secretaries in the Electrical Engineering Department, almost all of whom helped at one time or another with the typing.

To the many others in the Department and the Institute who gave me help, knowledge, or inspiration over the years, I offer my thanks, especially to Professor Charles Wilts, who provided me, perhaps without knowing it, with a model of integrity which I will not soon forget.

I gratefully acknowledge the financial support provided me by NASA, the Radio Corporation of America, and the Institute.

ABSTRACT

An experimental investigation of the optical properties of β -gallium oxide has been carried out, covering the wavelength range 220-2500 nm.

The refractive index and birefringence have been determined to about ± 1% accuracy over the range 270-2500 nm, by the use of a technique based on the occurrence of fringes in the transmission of a thin sample due to multiple internal reflections in the sample (ie., the "channelled spectrum" of the sample.)

The optical absorption coefficient has been determined over the range 220 - 300 nm, which range spans the fundamental absorption edge of β - Ga_2O_3. Two techniques were used in the absorption coefficient determination: measurement of transmission of a thin sample, and measurement of photocurrent from a Schottky barrier formed on the surface of a sample. Absorption coefficient was measured over a range from 10 to greater than 10^5, to an accuracy of better than ± 20%. The absorption edge was found to be strongly polarization-dependent.

Detailed analyses are presented of all three experimental techniques used. Experimentally determined values of the optical constants are presented in graphical form.

TABLE OF CONTENTS

	Acknowledgment	iii
	Abstract	iv
I.	Introduction	1
II.	Refractive Index	3
	A. Analysis of Technique	1
	B. Experimental Results	13
	C. Refractive Index for Another Propagation Direction	20
III.	Absorption Edge	23
	A. Transmission Measurement: Theory	23
	B. Transmission Measurement: Experiment	28
	C. Photocurrent Measurement: Theory	31
	D. Photocurrent Measurement: Experiment	36
IV.	Conclusion	46
	References	48
	Appendices	
	A. Details of Sample Thickness Calculation	50
	B. Determination of Hole Diffusion Length	52
	C. Sensitivity of Calculated α to Experimental Error	54
	D. Correction to Thickness Determination	56

I. Introduction

A. Background of this Investigation

Gallium oxide, β-Ga_2O_3, has been found[1] to be a semiconductor with a band gap of approximately 4.8eV. Its crystal structure has been exhaustively studied[2]; the crystal is monoclinic (space group C2/m), with one excellent cleavage along the (100) plane and a much poorer cleavage along the (001) plane. Reported optical investigations of β-Ga_2O_3 include a brief measurement of the absorption edge[3] and rather detailed studies of photo- and cathode- ray luminescence[4,5].

As reported by Lorentz,[1] the conductivity of β-Ga_2O_3 is dependent on the atmosphere in which it is grown (for flame-fusion grown crystals) or later annealed at high temperature. In an effort to further investigate this phenomenon, a study of the electrical properties of vacuum-deposited metal contacts on the (100) cleavage faces was begun. The current-voltage and capacitance-voltage characteristics, and zero-bias photocurrent as a function of wavelength were measured with several different metals including Al, Au, Pt and Cu, and barrier heights were determined from these data. (For details of these techniques, see the excellent review by C. A. Mead[6]). The barrier heights for Au and Pt were both approximately 1.35V, and those for other metals showed the linear correlation with electronegativity of the metal expected[7] for a highly ionic semiconductor. In particular, the Al-Ga_2O_3 barrier was sufficiently low to provide an ohmic contact at room temperature.

In the course of these electrical investigations it was realized that the combination of a wide-band gap semiconductor with the excellent

cleavage found in β-Ga_2O_3 afforded an opportunity for certain optical and electro-optical studies; these studies comprise the main topic of this thesis.

B. General Comments on Experimental Parameters

Because of the excellent (100) cleavage, it is very easy to produce optically flat plates of β-Ga_2O_3 with parallel faces and thickness ranging from <1μm to ~1mm. The experimental samples used in this work were all grown by flame fusion[8] in a slightly reducing atmosphere, and had electronic concentrations in the range of 0.5-$2 \times 10^{18} cm^{-3}$. Sample sizes were limited by the size of boules that could be grown, and the maximum dimension of any sample was <0.5cm; most were considerably smaller. All optical measurements, with one exception (see section II), were carried out with light propagating along the crystalline c-axis; that is, perpendicular to the easy cleavage described above. Most transmission measurements were performed in a Cary Model 14 UV/Visible/IR spectrophotometer; when polarized light was required, a Glan calcite-prism polarizer was used. The photocurrent measurements were made using a Gaertner quartz-prism monochromator along with the Glan polarizer; a chopped light source was used, and a P.A.R. lock-in amplifier was employed for photocurrent measurement.

II. Refractive Index

The refractive index of β-Ga_2O_3, for light incident parallel to the crystalline c-axis, was measured over the wavelength range 0.27-2.5 micrometers. The material was found to be birefringent: both principal values of refractive index and their difference were determined over this wavelength range. Because a rather unconventional measurement technique was used, an analytical discussion of this technique is presented first, followed by a description of the actual experimental parameters and results.

A. Analysis of Technique

The refractive index was determined from interference fringes ("channelled spectrum") observed in the optical transmission of a nearly transparent sample in the form of a flat plate with parallel faces; these fringes occur due to multiple internal reflections within the sample. The transmittance, for normally-incident light of wavelength λ, of a parallel-faced plate of material with complex refractive index $\hat{n} = n + ik$ and thickness d is[9]

$$T = \frac{16(n^2 + k^2)}{[(1+n)^2 + k^2]^2 \, e^{\frac{4\pi kd}{\lambda}} + [(1-n)^2 + k^2]^2 \, e^{\frac{-4\pi kd}{\lambda}} - 2[(1+n)^2 + k^2][(1-n)^2 + k^2] \cos\left(\frac{4\pi nd}{\lambda} + \delta\right)} \qquad (1)$$

(where δ is a function of k and n, of order k/10n for $k \lesssim n$).

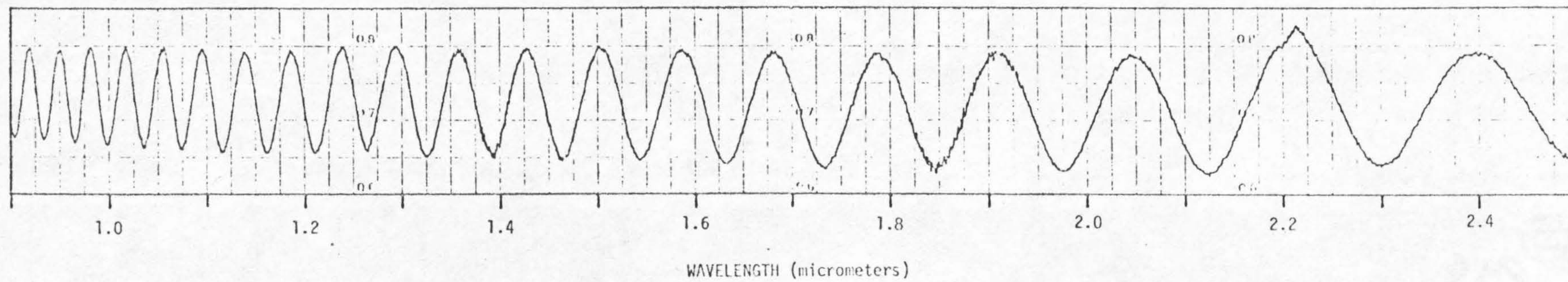

FIGURE 1. Example of Channelled Spectrum.

In the limit of negligible absorption ($k << n$ and $\frac{kd}{\lambda} << 1$)*, this equation reduces to

$$T = \frac{1}{1 + (\frac{n^2-1}{2n})^2 \sin^2 (\frac{2\pi nd}{\lambda})} \quad (2)$$

This form of the transmittance equation reveals the existence of periodic maxima and minima in T (i.e., interference fringes) as a function of λ according to the condition

$$\frac{2n(\lambda)\ d}{\lambda} = m \quad (3)$$

where m, the interference order, is integral for a transmission maximum and half-integral for a minimum.[10] An example of a transmission spectrum exhibiting such behavior is shown in Fig. 1. (The data shown are a plot of log T vs. λ made on a Cary Model 14 Spectrophotometer, with a sample of Ga_2O_3 of thickness 7.03 micrometers, approximately 1 mm x 3 mm in area).

While the value of refractive index as a function of wavelength is inherent in such a plot, as indicated by equation (3), there are practical difficulties in extracting it from the raw data. First, the sample thickness d must be determined; since it comes into equation (3) as a linear factor, the precision with which it can be determined directly limits the precision of the determination of n. Second, the

---

*This approximation is valid throughout the wavelength range used for this refractive index determination. See Section III.

continuity of the plot in Fig. 1 guarantees that we know the relative orders of all fringes detected, but provides no clue as to the absolute fringe order. That is, if the order of the first fringe (the one occurring at largest wavelength) is m_1, then we know that the order of the second fringe is

$$m_2 = m_1 + 1 \tag{4}$$

and similarly for all other fringes observed; however, the transmission plot does not unequivocally indicate the order of the first fringe. Hence, if some likely value M_1 is chosen (based, for example on some other estimate of refractive index), it may well be in error by some integer M_o. In that case all fringe orders will be in error by that same additive constant.

The first difficulty can be overcome for all samples if the thickness of any one sample can be independently determined by any method. Taking m to be a continuous function of wavelength, we can obtain $m(\lambda)$ for a given sample at any wavelength λ by interpolation from the integral values actually measured. Then, for two samples, I and II, of thicknesses d_I and d_{II}, and for any two wavelengths λ_a and λ_B, we have from equation (3):

$$m_I(\lambda_a) - m_I(\lambda_b) = 2d_I\left[\frac{n(\lambda_a)}{\lambda_a} - \frac{n(\lambda_b)}{\lambda_b}\right] \tag{5a}$$

and

$$m_{II}(\lambda_a) - m_{II}(\lambda_b) = 2d_{II}\left[\frac{n(\lambda_a)}{\lambda_a} - \frac{n(\lambda_b)}{\lambda_b}\right] \tag{5b}$$

and, by dividing (5b) by (5a),

$$\frac{d_{II}}{d_I} = \frac{m_{II}(\lambda_a) - m_{II}(\lambda_b)}{m_I(\lambda_a) - m_I(\lambda_b)} \quad . \tag{5c}$$

Since any additive error in fringe order will cancel in the subtractions, this equation yields the ratio of the two sample thicknesses directly from the data obtainable from a transmission plot like Fig. 1. (In practice the data from a number of wavelength points can be used in equation (5c) and the results averaged to obtain a more accurate value of the thickness ratio: see appendix A).

The second difficulty can be overcome if a sufficiently thin sample is available. If, for a given sample, an arbitrary order assignment is made, as discussed above, we have a set of wavelengths λ_i, at which fringes occur, and associated with each fringe a relative order M_i which differs from the actual absolute fringe order m_i by some unknown M_o. That is

$$m_i = M_i + M_o \tag{6}$$

for all fringes i. Then, noting that equation (3) can be solved to yield

$$n(\lambda_i) = \frac{m_i \lambda_i}{2d} \tag{7}$$

at each fringe, we can define a "pseudo-index" $N(\lambda)$ based on the <u>assigned</u> orders M_i:

$$N(\lambda_i) \equiv \frac{M_i \lambda_i}{2d} = n(\lambda_i) - \frac{M_o \lambda_i}{2d} \tag{8}$$

This "pseudo-index" of refraction corresponds to a family of curves, represented schematically in fig. 2, with the unknown integer "offset" M_o (or, correspondingly, the known choice of 1st-fringe order, M_1) as a parameter. One of these curves, the one for which $M_o = 0$, is the true refractive index; the others differ from it at any wavelength λ by $M_o\lambda/2d$. For sufficiently thin samples the linear dependence of this error term on λ will overwhelm the actual variation of refractive index with λ; then the curve next above the correct $n(\lambda)$ will show a dispersion of the wrong sign ($N(\lambda)$ increasing with λ) while the next lower curve will pass below $N(\lambda) = 1$. Since both of these conditions are impossible on basic physical grounds, the actual refractive index, lying between the two $N(\lambda)$ choices just discussed, will be unequivocally indicated.

One other test for the correct choice of absolute fringe order exists, if several samples of differing thicknesses are available. For each sample, we can plot a family of $N(\lambda)$ curves like the set shown in fig. 2. One curve of each set is the actual refractive index $n(\lambda)$, and this curve should be the same for all samples. Thus if the $N(\lambda)$ families for two samples are superimposed, one curve from one family and one from the other should coincide, these being the correct refractive index, for which in both cases $M_o = 0$. The next curve up in each of the two families will be spaced from $n(\lambda)$ by $\frac{\lambda}{2d}$; since the thickness of the samples are presumed different, the spacings will also differ, and the next curves up and down will not coincide. If the sample thicknesses are not rationally related, in fact, <u>no</u> $N(\lambda)$ curves other than those for which $M_o = 0$ will coincide. Thus again, the actual $n(\lambda)$ curve is unambiguously selected.

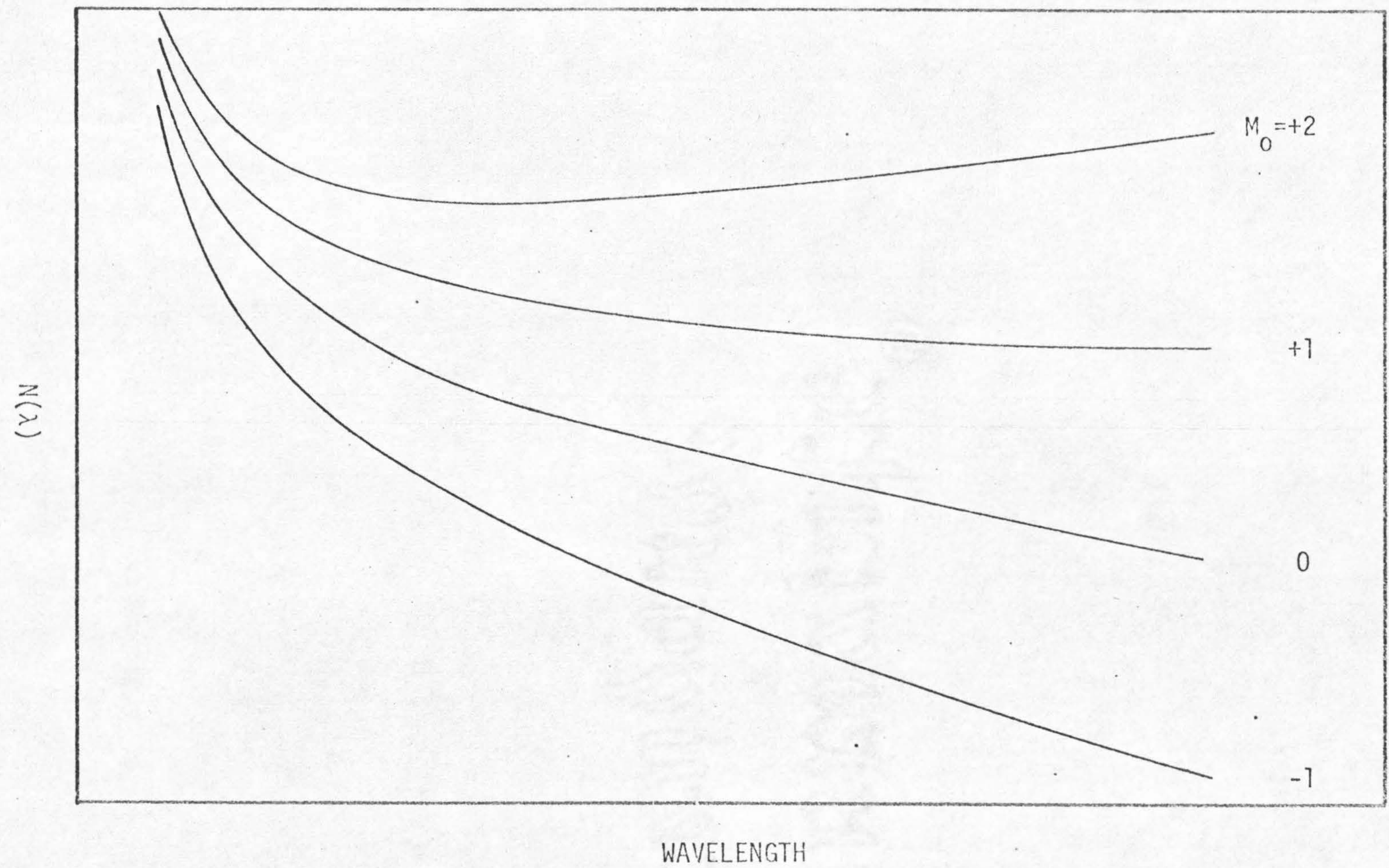

FIGURE 2. Schematic example of "pseudo-refractive index" vs. wavelength for several choices of initial order.

In the case of a birefringent material, an additional feature arises in the channelled spectrum: if unpolarized light is used in the transmission measurement, the observed fringes will exhibit a superimposed pattern of "beats". Fig. 3 is an example of part of a channelled spectrum showing such beats.

This effect can be understood in terms of the nature of electromagnetic wave propagation in an anisotropic crystal. In such a crystal (assumed to be lossless), for a given direction of propagation, exactly two independent waves may propagate, each linearly polarized and with their two $\vec{D}$ vectors at right angles; they will, in general be characterized by two differing refractive indices.[11]* If light incident on the crystal is either unpolarized or polarized along any direction other than the two allowed directions of polarization, it will be split into two beams propagating at different velocities (i.e., affected by differing refractive indices). Because the refractive indices affecting the two beams are different, the fringes in transmitted intensity of the two beams will have different periods in $1/\lambda$ (see eqn. (2)). When total transmitted intensity is measured, the two sets of fringes, corresponding to orthogonally polarized beams, will add linearly; since their periods in $1/\lambda$ are slightly different, they will alternately cancel and reinforce each other. The total transmitted intensity, therefore, will show fringes with beats. Recalling the

---

*If the propagation direction is parallel to one of the three principal axes of the permittivity tensor which connects $\vec{E}$ and $\vec{D}$ in the crystal, then the two allowed polarizations will be parallel to the other two principal axes of the permittivity, and the associated refractive indices will be two of the three principal refractive indices of the crystal.[11] In the present case this condition is satisfied, for the crystalline

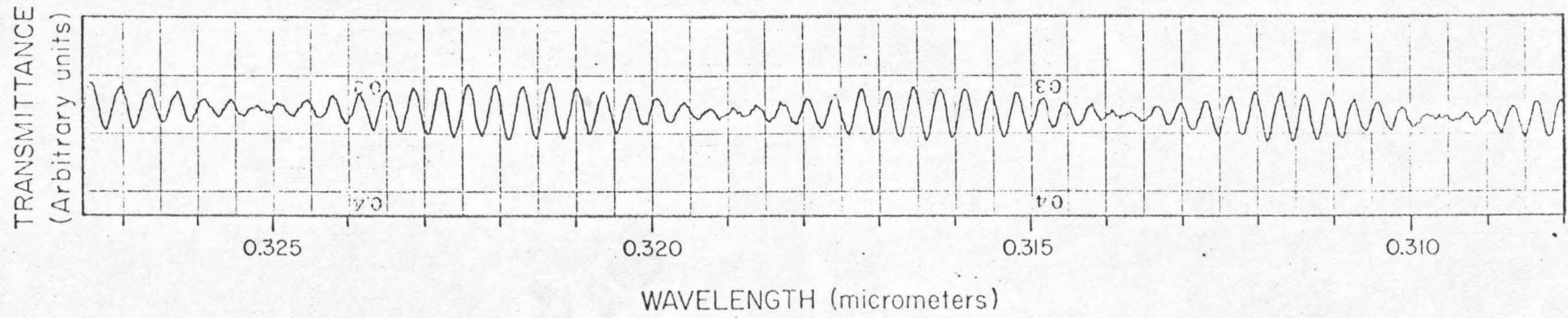

FIGURE 3. Example of channelled spectrum showing beats due to birefringence.

relationship between fringe order, wavelength, refractive index and thickness which was derived earlier (eqn. (7)), we can see that for each of the two independent polarizations (referred to here by the subscripts 1 and 2), fringes obey the conditions .

$$n_1 = m_1\lambda_1/2d \tag{9a}$$

$$n_2 = m_2\lambda_2/2d \tag{9b}$$

Thus at a particular wavelength λ where a fringe reinforcement or cancellation (beat maximum or minimum) is observed, we must have

$$\Delta n \equiv n_1 - n_2 = (m_1 - m_2)\frac{\lambda}{2d} \equiv \frac{\Delta m\lambda}{2d} \tag{10}$$

with Δm an integer for reinforcement and half-integer for cancellation. This equation, in obvious analogy to equation (3), gives us birefringence Δn as a function of wavelength from the wavelengths at which beats occur in the channelled spectrum.

An alternative method of determining birefringence, which is also capable of identifying the crystalline directions associated with the larger and smaller refractive indices, is the use of polarized light for the transmission measurement. According to the above analysis, an incident beam which has one of the two polarizations permitted to propagate in the crystal will be propagated as a single beam, and will emerge displaying a fringe system without beats, and characterized by a single refractive index. Thus by experimentally determining the two directions of polarization of incident light (with respect to the crystalline axes)

---

c-axis, which is the direction of propagation in all but one of the measurements performed in this work, is also a principal axis of the permittivity tensor.[12]

for which no beats occur, one can determine the directions in the crystal along which the principal axes of the permittivity lie, and the principal values of refractive index which correspond to them.*
Birefringence can be calculated from such data, being simply the difference of the two principal refractive indices at each wavelength.

B. Experimental Results

In the present work, the optical transmission of a number of samples, ranging in thickness from 0.86 to 55.3 μm, was measured over the wavelength range 0.27 to 2.5 μm. The transmission spectra of all samples exhibited the interference fringes described in part A; five samples, spanning the thickness range, were selected for detailed analysis. For the purposes of the following discussion, they will be identified as:

No. 1:	thickness	34.27	micrometers
No. 2:	"	7.031	"
No. 3:	"	0.860	"
No. 4:	"	1.21	"
No. 5:	"	55.35	"

For these samples, transmission was measured using both unpolarized

---

*Beats in the transmission fringe system could also occur if the sample whose transmission was being measured had a step separating two areas of uniform but differing thickness. Beats due to such a cause would not, however, depend at all upon the polarization of the incident beam; hence the experiment just described would reveal such a thickness step.

light, over the entire wavelength range, and polarized light* over the range 0.27 to 2.1 μm. The measurements were all made using the Cary Spectrophotometer. The wavelengths of occurrence of all fringes, both maxima and minima, were determined for all samples.

Sample thicknesses were calculated on the basis of equation (5c) using the procedure explained in detail in Appendix A; the single independent thickness determination required was performed on sample No. 1 using X-ray absorption, by the following procedure. A metal mask of sufficient thickness to completely absorb the CuKα radiation employed was prepared, with an aperture which could be completely covered by sample No. 1. Transmitted X-ray intensity was measured with and without the sample present across the aperture. Using the known[2] absorption coefficient of 299 cm^{-1} of β-Ga_2O_3 for CuK_α radiation, the sample's thickness was calculated to be 34.27 ± 0.10 micrometers. (The probable error is based on X-ray counting statistics). Since this measurement is the basis of all thickness values used in this work, the probable error assigned above, amounting to ± 0.3%, applies to the entire refractive index determination.

The experimental transmission spectra obtained differ in one respect from the theoretical form of eq. (2): due to the finite wavelength resolution of the spectrometer and to the convergence of the beam at the sample, a slight "averaging" over λ and d occurs, with the result that fringe amplitude is not as great as that predicted by Eq. (2). Thus

---

*Polarized light was not used with samples No. 3 and 4 for reasons explained below.

the fringe amplitude cannot be used as an independent measurement of n.

As discussed in part A of this section, it is necessary, in order to use the transmission fringe data to calculate refractive index, to determine for some sample the absolute order of the observed fringes. The method, described there, of plotting against wavelength the "pseudo refractive index" resulting from various probable choices of order, was applied to both samples No. 3 and No. 4. The resulting plots are displayed in Fig. 4a. (The experimental data shown here are in exact analogy with the hypothetical data shown in Fig. 2). The upper curves for both samples, and the lower one for No. 3, can be ruled out on the basis of non-physical behavior, as discussed in part A of this section; in addition, the two samples yield a coincidence only for the center choice for each. Thus, both criteria described in part A indicate the center curve to be the actual refractive index $n(\lambda)$. In fig. 4b, the central set of data from fig. 4a is replotted on an expanded refractive index scale, along with the three adjacent $N(\lambda)$ curves for sample No. 2 which bracket it. The spacing between adjacent $N(\lambda)$ curves for sample No. 2 is much smaller than that between the $N(\lambda)$ curves for either sample No. 3 or No. 4, due to the much greater thickness of sample No. 2. By the argument just employed, the $N(\lambda)$ curve for sample No. 2 which matches the $n(\lambda)$ values from No. 3 and 4 must be the $M_o = 0$ choice for that sample; even with the considerable scatter of the data from the thinner samples, the choice for No. 2 is unambiguously the center one shown.

The scatter in the data from the thinner samples is due to their extremely small area (6×10^{-4} cm^2 and 2×10^{-3} cm^2 for No. 3 and No. 4, respectively) which limited transmitted light sufficiency to make their

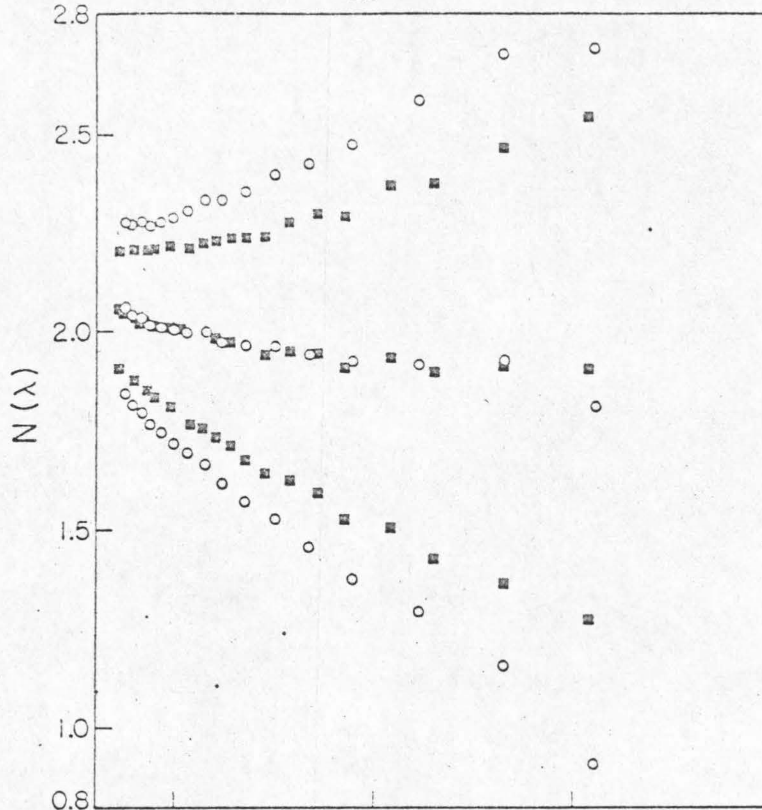

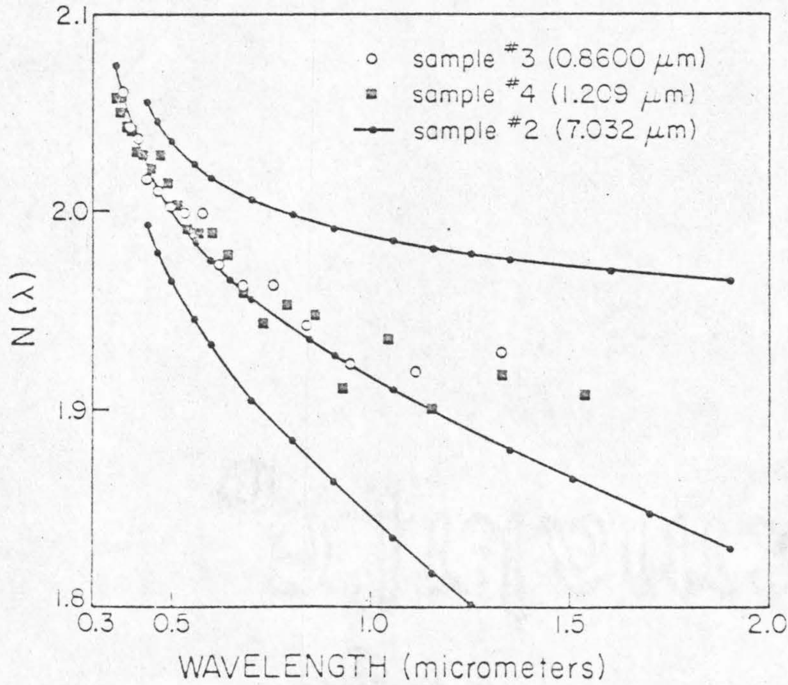

FIGURE 4. A) "Pseudo-refractive index" for the two thinnest samples, with three adjacent choices of initial fringe order. B) Equivalent data from sample No.2, with central data from(A) superposed.

spectra very noisy. This noise led to difficulty in assigning an accurate wavelength to each fringe, and thus to the scatter in n(λ) which is seen in fig. 4. Sample No. 2 (as well as No. 1 and No. 5) are large enough to provide spectra with negligible noise, and therefore very scatter-free N(λ) curves. Therefore, once the choice of M_1 was made for sample No. 2 as described above, no difficulty was encountered in correspondingly choosing for the thicker samples.

Unpolarized light, yielding an n(λ) which is an average over birefringence, was used for the above data because the loss of 1/2 in intensity due to a polarizer made measurements on samples No. 3 and No. 4 unusably noisy. However, with the thicker and larger-area samples, the intensity loss was tolerable, and a Glan calcite-prism polarizer was used in the wavelength range 0.27 - 2.1 micrometers to resolve the principal refractive indices. Beyond 2.1 micrometers, transmittance of the polarizer became too irregular with wavelength to permit transmitted intensity variations due to interference in the sample to be distinguished; hence unpolarized light was used in this region for all samples.

The crystalline directions associated with the principal refractive indices were found using the procedure described in part A of this section: the polarizer was rotated with respect to the sample, until a direction was found for which no beats occurred in the channelled spectrum. Because no precise angle-measuring apparatus could be installed in the sample chamber of the Cary Spectrophotometer, and because the no-beat condition is not sharply defined, then directions are known to only about ± 10°. Within that accuracy the principal directions were found to be parallel to and perpendicular to the

crystalline b-axis.

In monoclinic crystals the directions of the principal axes of permittivity may in general vary with wavelength; that is, the crystal may exhibit axial dispersion.[13] In the present instance, the directions indicated by the beat-elimination procedure were constant over the wavelength range (0.28 μm to 0.43 μm) where beats occurred in the thickest sample used. In order to ascertain the directions of the principal axes for wavelengths larger than 0.43 μm, use was made of the fact that light propagating with polarization other than one of the allowed directions (in this case, the principal directions) should show a channelled spectrum corresponding to some "average" refractive index between the two principal values. For this reason, a polarization direction which yields a value of $n(\lambda)$ which is either a maximum or minimum at a given wavelength must be one of the two allowed (principal) directions. The principal directions were determined using this criterion at $\lambda = 1.95$ μm, and were found to be identical to those found in the $\lambda < .43$ μm region, to within ± 10°.

With the directions of the principal refractive indices thus established, $n_{\parallel}(\lambda)$ and $n_{\perp}(\lambda)$ (the subscripts referring to the crystalline b-axis) were measured from $\lambda = 0.27$ μm to $\lambda = 2.1$ μm on samples No. 1 and No. 2. The "average" refractive index resulting from unpolarized light was measured out to $\lambda = 2.5$ μm. The results of these measurements, which constitute the final results of this refractive index determination, are plotted in fig. 5. Data from both samples are plotted; they are not distinguished, since they match to within the resolution of this plot, which is considerably less than the absolute probable error of the measurement.

As explained in part A of this section, birefringence can be

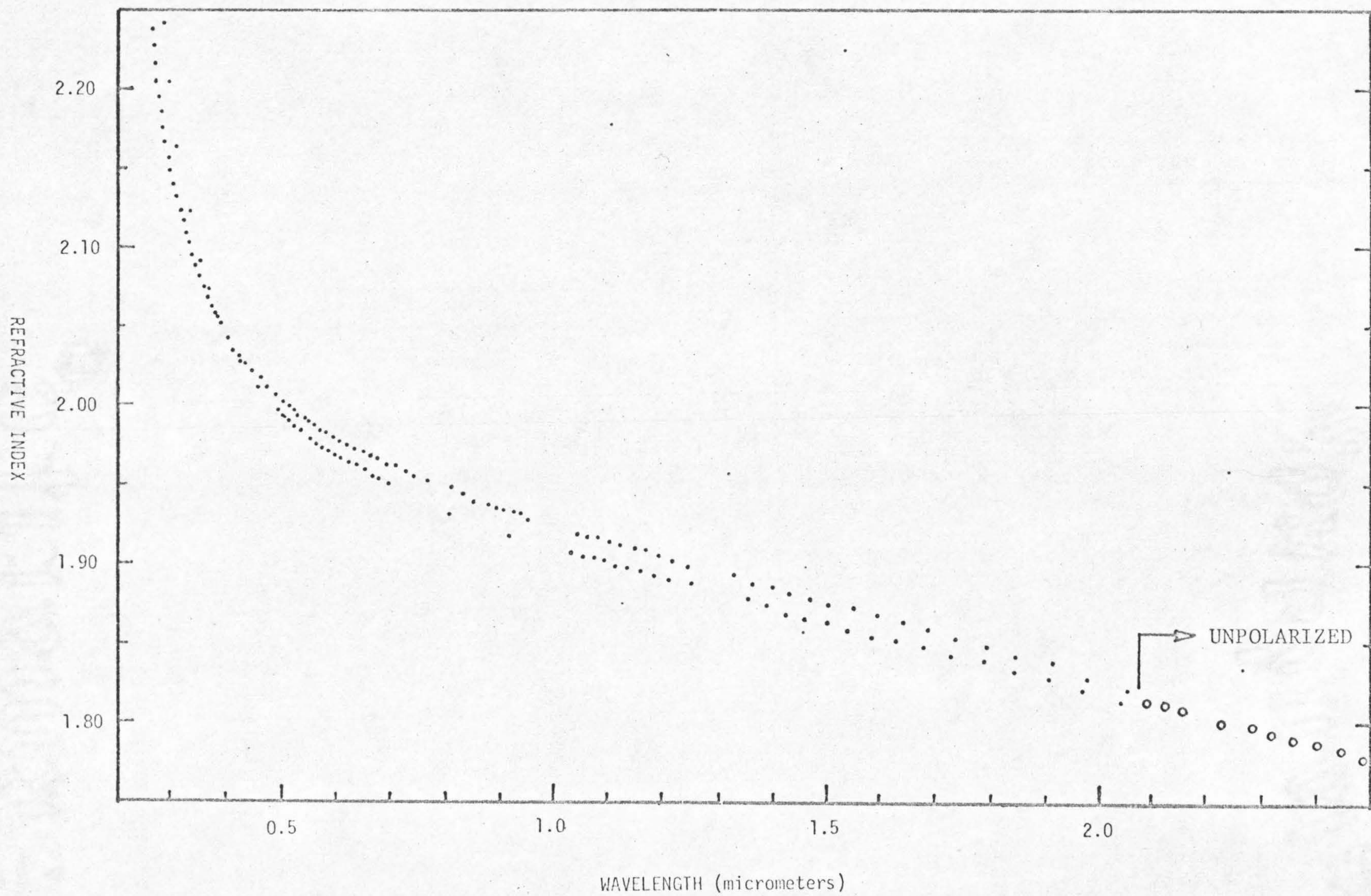

FIGURE 5. Refractive index of Ga_2O_3 vs. wavelength.

determined from the wavelengths of occurrence of "beats" in fringe systems obtained with unpolarized light, as well as directly from the polarized-light of fig. 5. Such "beat" data from two samples is considered here: samples No. 2 and 5. Only one fringe cancellation occurred in the spectrum of sample No. 2 before the absorption edge was reached: it occurred at 0.3225 micrometers. Since no cancellation occurred at longer wavelength, this one must correspond to the lowest fringe order difference capable of yielding a cancellation: $\Delta m = 1/2$.

The first cancellation in the spectrum of sample No. 5 occurs at 0.41325 μm, and the second at 0.37585 μm. It can be seen in fig. 5 that the two principal refractive indices cross over between these two w velengths; hence, $|\Delta m|$ in <u>both</u> cases must be 1/2; (the order difference, of course, changes sign). Subsequent cancellations were assigned order differences of 3/2, 5/2, etc. The resulting values of Δn calculated from eq. (10) are plotted in fig. 6. This figure shows $n_{\perp} - n_{\parallel}$ calculated from the data shown in fig. 5 (solid dots) along with Δn derived, as just explained, from the beat data (open points). The two sets of data are seen to be in substantial agreement.

C. Refractive Index for Another Propagation Direction

In β-Ga_2O_3, the cleavage perpendicular to the c-axis is the only one which yields surfaces of sufficient perfection for interference measurements of the type just described. However, a minor cleavage exists along the (001) planes, and a sample was produced which had two reasonably flat faces along these planes, over an area about 0.02 mm square. An extremely sharp grid of lines was viewed through the sample (looking through the (001) faces) under a microscope, and the sample

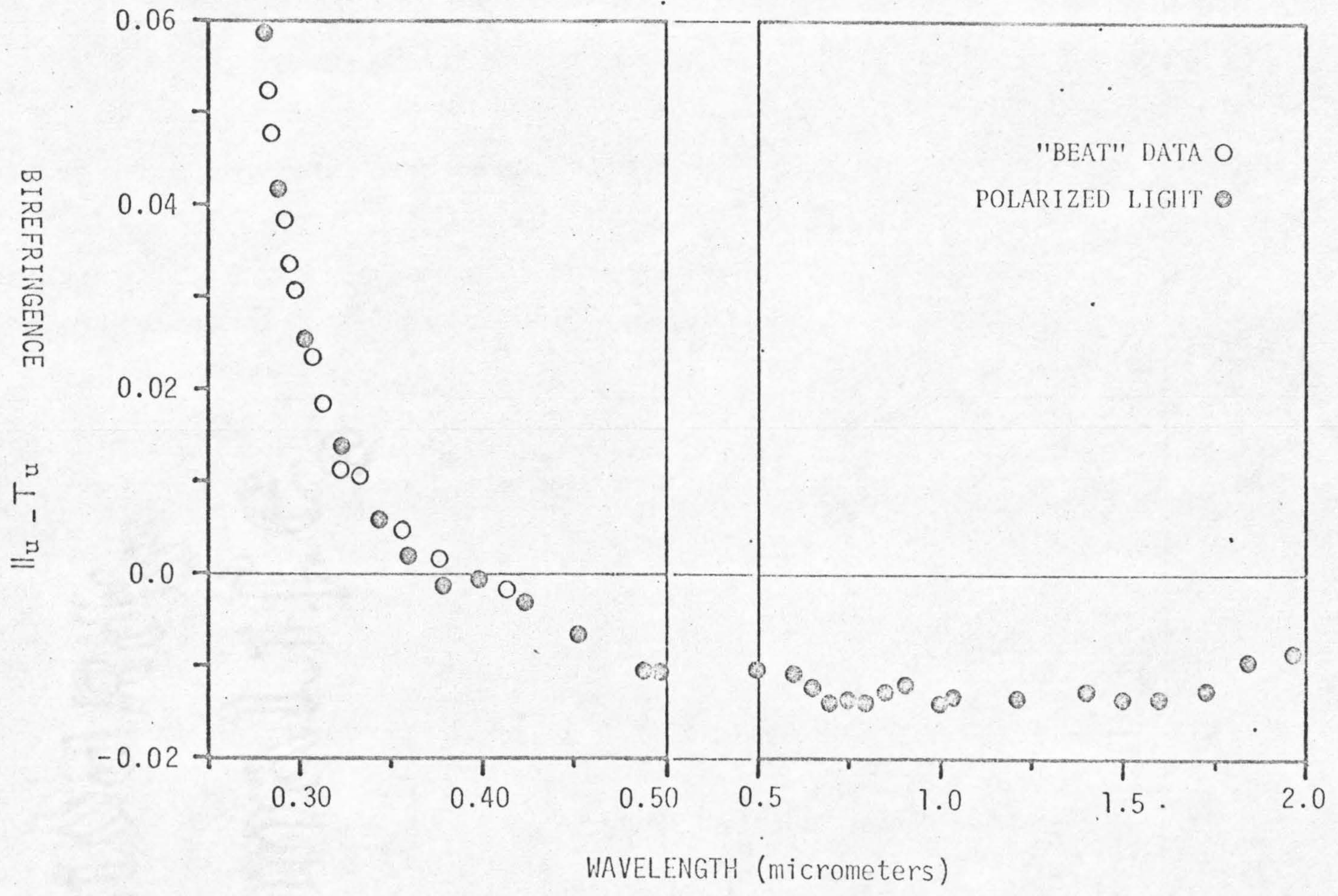

FIGURE 6. Birefringence of Ga_2O_3 vs. wavelength.

rotated. If the sample exhibited birefringence for light propagating in this direction, the image of the grid should show splitting; this was not detectable. For comparison, the same sample held so that the view was along the c-axis showed very obvious splitting of the image. It is estimated on this basis that birefringence for light propagation perpendicular to (001) planes is $\Delta n < .002$ at $\lambda \sim 0.5\mu m$.

III. Absorption Edge

The optical absorption of β-Ga_2O_3 was investigated in the vicinity of a strong absorption edge at about 4.8 eV (0.25 μm) which has previously[3] been associated with the electronic bandgap of the material. In this investigation two experimental techniques were used: (1) a conventional measurement of the transmittance of a plate of the material as a function of wavelength of incident light, which is a direct measurement of the optical absorption coefficient α, and (2) measurement of short-circuit photocurrent generated by light incident on a Schottky surface-barrier fabricated on the material, from which α can be inferred if the optical absorption is assumed to be due to an electronic valence-to-conduction-band excitation.

In parts A and C below, these two experimental techniques will be described and analyzed, and in parts B and D the respective experimental results will be presented and discussed.

A. Transmission Measurement: Theory

This measurement can be regarded as an extension of the measurement discussed in Section II into a wavelength range where the conditions assumed there, $k \ll n$ and $kd/\lambda \ll 1$, no longer apply. Equivalently, one may say that absorption, as well as reflection, contributes to the difference between incident and transmitted intensity.

Although the approximation made in simplifying equation (1) to obtain equation (2) is not valid here, another approximation can be used. Most samples used in this determination of α were sufficiently

thick that the "averaging" of the argument of the cosine term in equation (1) due to beam convergence and spectrophotometer resolution completely washed out the interference fringes discussed in Section II. This effect can be taken into account theoretically by finding an "average" value of the transmittance expressed by equation (1): specifically, the integral of T over one cycle of the cosine term, divided by 2π, is such an average. Performing the indicated integral (a standard form) yields the average, or "smeared" transmittance at a wavelength λ:

$$\overline{T} = \frac{16(n^2 + k^2)}{[(n+1)^2 + k^2]^2 \, e^{4\pi kd/\lambda} - [(n-1)^2 + k^2]^2 \, e^{-4\pi kd/\lambda}} \qquad (11)$$

(This expression will be used in evaluating transmittance data even from samples which do exhibit fringes at or beyond the absorption edge; for such samples the experimental "average transmittance" will be taken as the midline through the rapid fluctuations of T due to interference. Even for the thinnest sample used in this determination of α, the error in α resulting from this procedure is estimated to be less than one percent.)

Equation (11) gives the transmittance of an ideal uniform sample in a uniform beam, in terms of the sample refractive index and extinction coefficient, and the wavelength. However, the actual experiment is carried out with a sample of finite size in a non-uniform spectrophotometer beam. Thus, equation (11) must be modified to include these aspects of the experiment, in order to adequately analyze the experimental data.

Since the spectrophotometer beam was much larger in area than any available samples, it was necessary to mask the beam to the sample size and shape; in addition several samples had imperfections (bubbles and other inclusions) which effectively masked additional beam area and subtracted from incident intensity. This situation is depicted in Fig. 7. In order to take into account the losses of beam power (which is the quantity actually measured in the spectrophotometer) due to the opaque parts of the mask and sample, or, in other words, to establish a baseline for the transmittance measurement, the power transmitted through the sample-plus-mask structure was measured in a wavelength range where absorption contributed negligibly to beam power losses. At such wavelengths the average transmittance given by equation (11) reduces to the simple limiting form

$$\overline{T} = \frac{2m}{n^2 + 1} \qquad (12)$$

which can be evaluated at the wavelengths of interest by using the $n(\lambda)$ data from Section II. In the more general case of equation (11) as well as the limit of equation (12), the ratio of power transmitted by the sample-mask structure to incident power, here labelled sample transmission $\mathcal{T}$, will be smaller than the ideal sample transmittance $\overline{T}$ by a multiplicative constant γ which accounts for the occluded beam area. Since $\mathcal{T}$ can be measured, and $\overline{T}$ calculated, at wavelengths where absorption is negligible, (and equation (12)

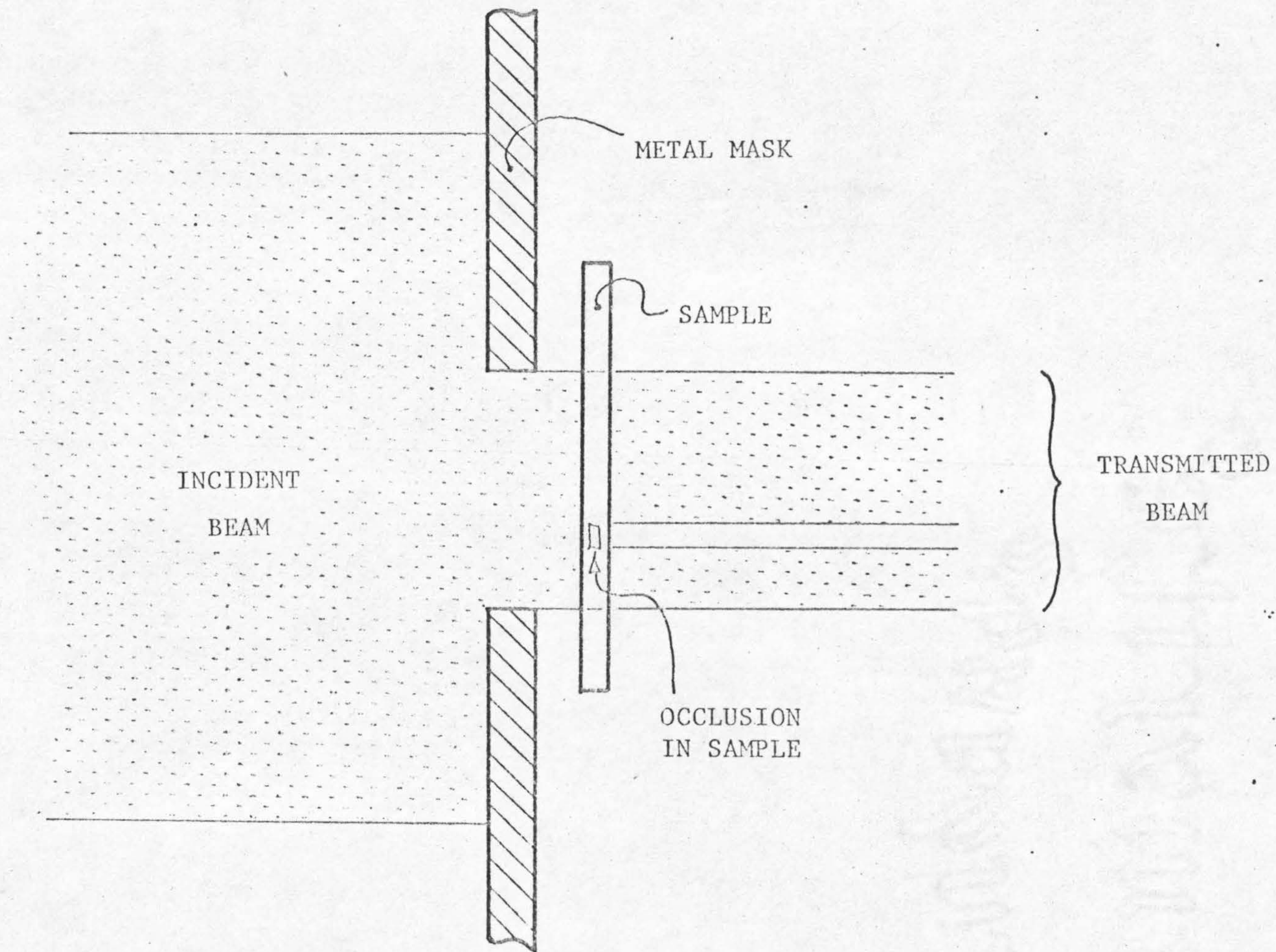

FIGURE 7. Schematic representation of sample and beam geometry in transmission measurement.

accordingly applies), γ can be determined for each sample.* We then have, for all wavelengths, the sample transmission given by:

$$T(\lambda) = \frac{16\gamma(n^2 + k^2)}{[(n+1)^2+k^2]^2 e^{4\pi kd/\lambda} - [(n-1)^2+k^2]^2 e^{-4\pi kd/\lambda}} \qquad (13)$$

Having experimentally determined γ for a given sample, and measured T over the wavelength range in which sample absorption is to be determined, it is necessary to apply equation (13) to the experimental data in such a way as to extract a value of $\alpha(\lambda)$, the quantity sought. The extinction coefficient k is the only unknown in equation (13); since this equation is transcendental, it was decided to extract k by an iterative procedure. Newton's method was chosen, as being the simplest method available, and quite adequate to the computation. Finally, α was calculated from k using the definition

$$\alpha \equiv \frac{4\pi k}{\lambda} \qquad (14)$$

This determination of α becomes uncertain in two limits.
(1) $\alpha d \ll 1$. In this case, the absorption is negligible compared to reflection and other beam power losses; hence, a slight error in $n(\lambda)$ or γ, for example, will produce a large error in the calculated

---

*The value of γ actually depends on the position of the sample in the spectrophotometer beam, since the intensity profile of the beam is not uniform. However, the transmission measurements used to calculate γ and α were carried out as a single experimental "run" with the sample fixed in position in the spectrophotometer during the entire measurement. Therefore the calculated value of γ is applicable to the calculation of α.

value of α .

(2) $\alpha d \gg 1$. In this case, nearly all the light entering the sample is absorbed, and scattered light in the spectrophotometer and sample fluorescence become important in comparison with transmitted light, leading to an apparent reduction of α below its actual value. In order to obtain values of α over an appreciable range, it is therefore necessary to employ several samples of differing thickness, each contributing values of α around the point $\alpha \simeq 1/d$.

By choosing sample thicknesses appropriately, a continuous reliable curve of α vs λ can be obtained over a considerable range in α .

B. Transmission Measurement: Experiment

Four samples were used in this measurement, with thicknesses as follows:

No. 1:	thickness	34.27 μm
No. 2:	"	7.031 μm
No. 6:	"	419.6 μm
No. 7:	"	942.7 μm

The first two samples were used also in Section II of this work and the method used to determine their thicknesses is described there. The thicknesses of the other two samples were measured using an "electronic micrometer," a mechanical micrometer equipped with a spherical anvil (of radius ∿0.5 mm) and an electronic strain sensor for detecting contact with the sample. The value of thickness obtained with this

apparatus is estimated to be accurate to ± 2 μm.

In the transmission measurements on these samples, the procedure described in part A above was used. Each sample, mounted on a metal mask which passed light only through the usable area of the sample, was held rigidly in the spectrophotometer beam, with a Glan prism mounted just ahead of it in the beam. The transmission of this combination was measured from about 4000Å to a wavelength sufficiently short that the transmitted beam power was too small for the spectrophotometer to detect. (This cutoff wavelength varied with sample thickness.) These raw transmission data were first normalized by the measured transmission of the Glan prism alone, which also took into account any baseline irregularity of the spectrophotometer itself. The normalized transmission from 4000Å down to the onset of strong absorption (between about 2900Å and 2550Å for the various samples) was used, together with the refractive index data reported in Section II, to calculate the effective ratio of sample area to beam area γ . Then the remainder of the transmission data, in conjunction with γ and the known refractive index*, were used in the solution of equation (13) for $k(\lambda)$. Finally, $\alpha(\lambda)$ was calculated using equation (14).

The results of the measurements are shown in Fig. 8. Two curves of α vs $h\nu$ are shown, as it was found that α depended on the

---

*In the case of sample No. 2, the measured refractive index data had to be extrapolated in order to complete the calculation of α at the shortest wavelengths usable. Since T depends exponentially on αd and only linearly on n , the error from this extrapolation is negligible for values of $\alpha d \gtrsim 1$.

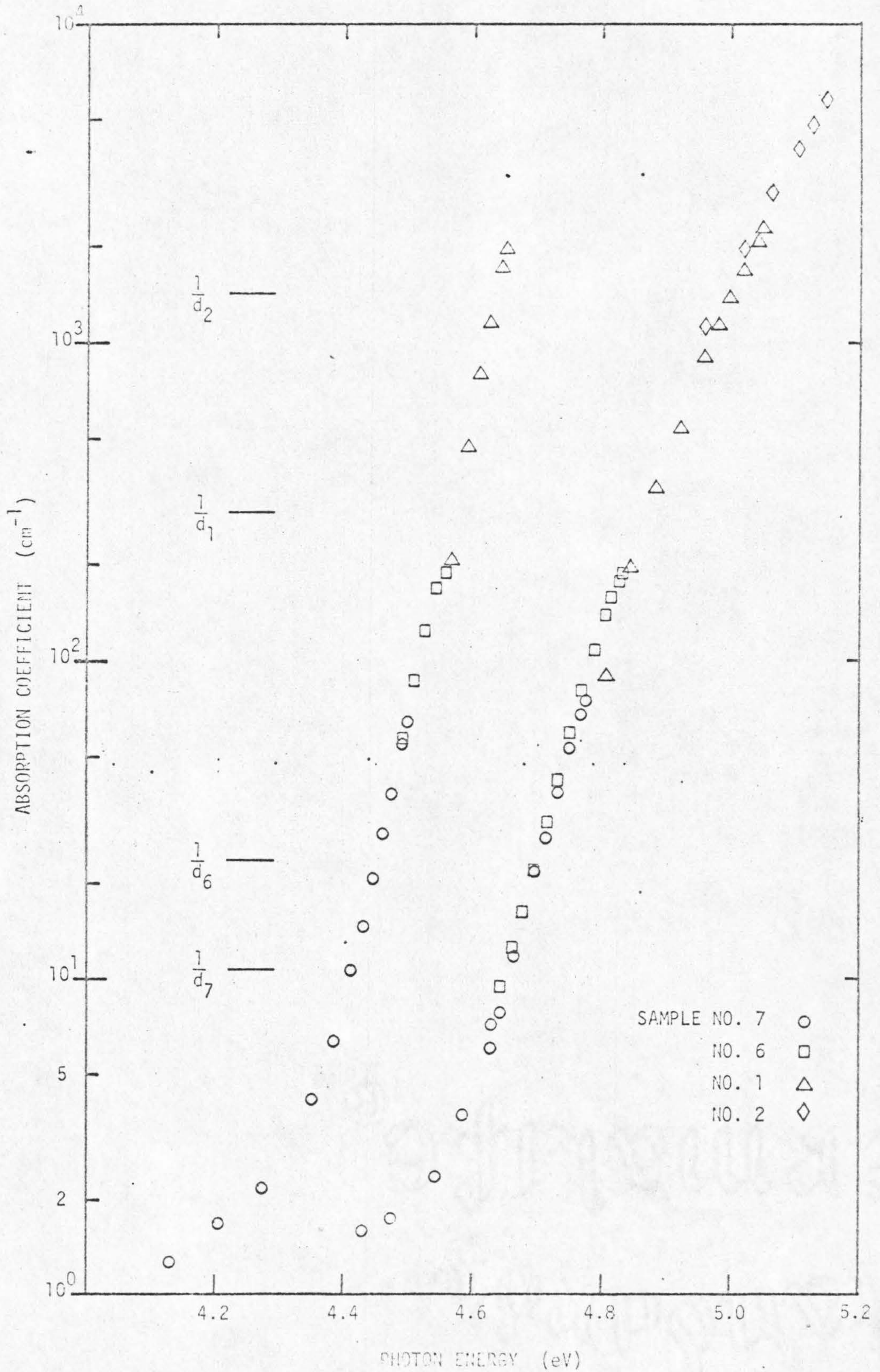

FIGURE 8. Absorption coefficient v. wavelength, from transmission.

polarization of the incident light with respect to the crystalline axes. Specifically, it was found that unless polarization was oriented either parallel or perpendicular to the crystalline b-axis (within about $\pm 5^{o}$) the absorption edge exhibited a shoulder due to the absorption of essentially all light of one polarization before any light of the other polarization was absorbed.* Thus two characteristic directions of polarization for absorption were found, which are in fact coincident with the optic axes found in the refractive index determination (see Section II). The values of α vs. $h\nu$ for these two directions are the ones shown in Fig. 8.

Points from the four samples are distinguished in Fig. 8, showing the range of values of α contributed by each sample. In addition, the reciprocals of the four sample thicknesses are indicated. As expected from the discussion in part A above, of the limitations on the α determination at the limits $e^{\alpha d} \to 1$ and $e^{\alpha d} \ll 1$, the reciprocal thickness of each sample falls approximately in the middle of the range of α values contributed by that sample.

C. Photocurrent Measurement: Theory

If the absorption edge being investigated is in fact due to the electronic bandgap of $\beta\text{-}Ga_2O_3$, then each photon absorbed by the crystal in this wavelength range should result in an electron being excited from a state in the valence band to one in the conduction band. If a means can be provided for collecting these optically-excited

---

*This shoulder was observed by Tippins[3] who used unpolarized light in his transmission measurement, but the polarization-dependence of the absorption edge was not recognized in that work.

electrons, then the absorption of light by the crystal can be measured indirectly, by measuring photocurrent.

A Schottky barrier formed on the surface of the sample by the disposition of a layer of metal is one means of collecting photo-generated electrons. The properties of such surface barriers have been reviewed in detail[6]; the relevant points will be briefly mentioned here.

The energy-band diagram of a metal-semiconductor surface barrier (Schottky barrier) is shown in Fig. 9a, and the corresponding physical structure in Fig. 9b. The structure is depicted for the condition of zero applied bias, in other words, at equilibrium. The conduction and valence bands of the semiconductor, and the Fermi energy (which is constant throughout the structure) are labeled; the semiconductor is represented as strongly n-type. The important features of this structure for the present discussion are the potential barrier of height ϕ_B between the semiconductor and the metal, and the "depletion layer" which extends from the metal-semiconductor interface to a depth w into the semiconductor. The depletion layer is characterized by the absence of mobile charge carriers (and the corresponding presence of a fixed space charge due to ionized donors) and the existence of a permanent "built-in" electric field of such a sense as to drive electrons from the surface into the semiconductor.

If an electron is excited from the valence band of the semiconductor to the conduction band within the depletion layer, it will be prevented from entering the metal by the potential barrier, and will be driven into the neutral semiconductor by the built-in electric field.

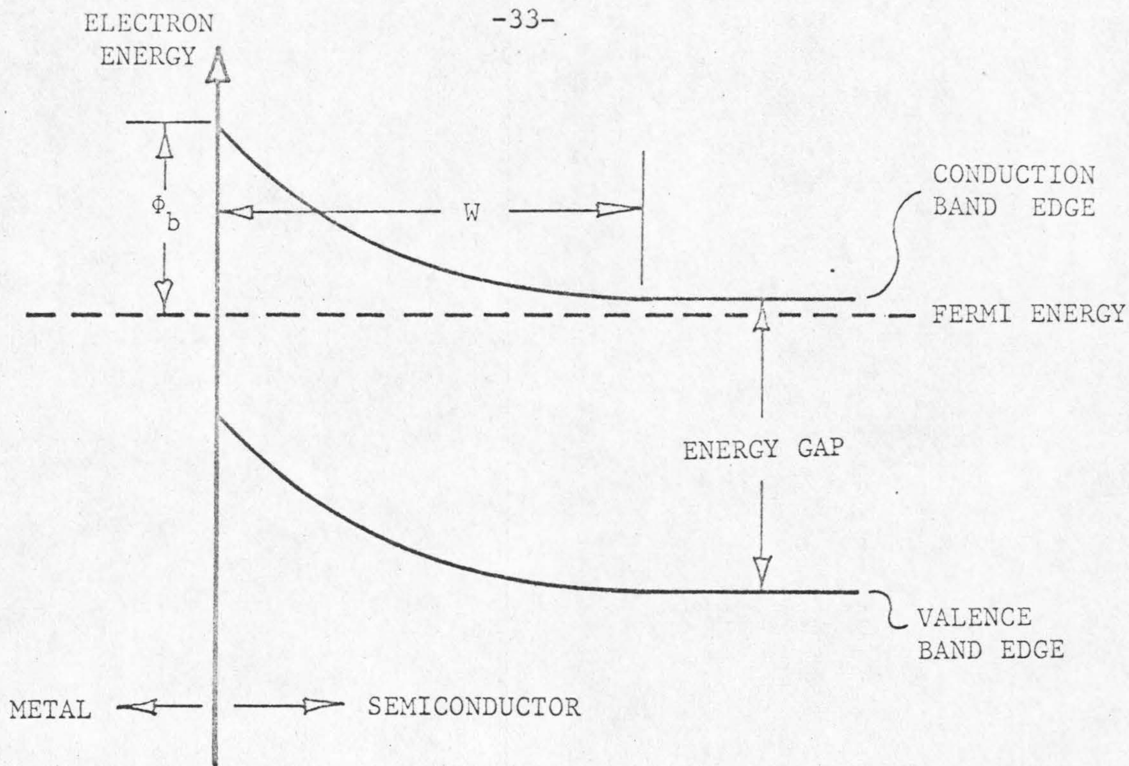

(A)

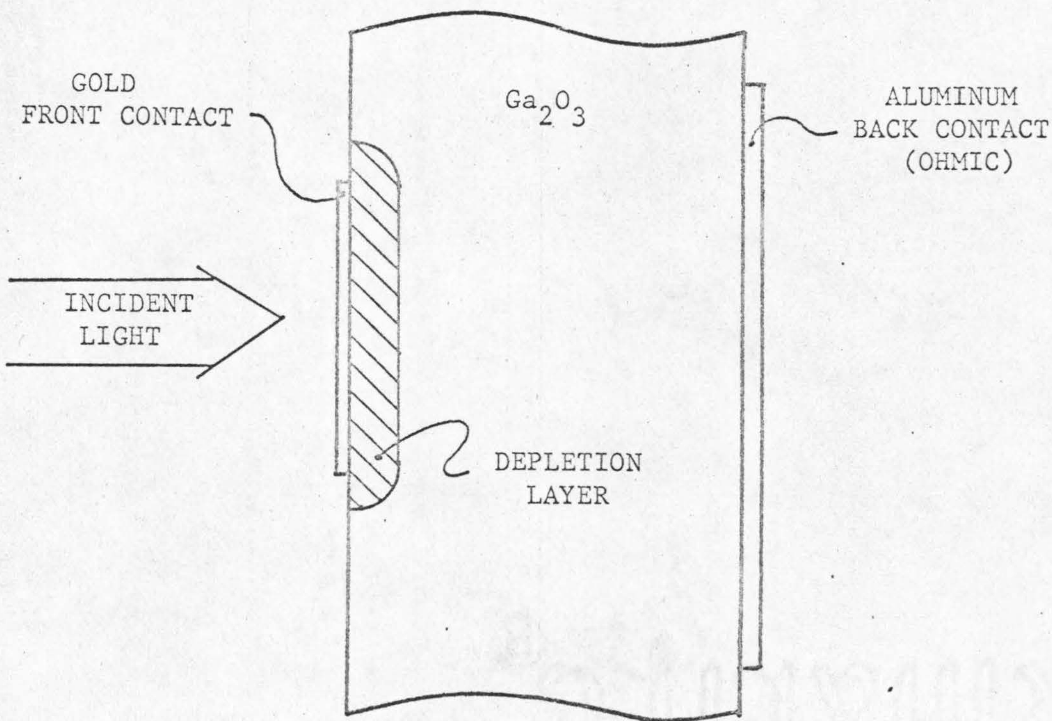

(B)

FIGURE 9. A) Energy-band diagram of Schottky barrier. B) Sample geometry.

The corresponding hole produced in the valence band will be driven toward the metal. The net effect is the passage of one electronic charge from the metal side to the semiconductor side of the experimental structure. Once in the neutral (conductive) portion of the semiconductor, the electron may be considered to flow through the external circuit back to the metal layer, in order to maintain zero voltage across the structure. Thus the absorption of one photon within the depletion layer results in the passage of one electronic charge through the external circuit.

If such an electronic excitation occurs within the neutral bulk of the semiconductor, the excited electron, prevented by the barrier from entering the metal, will simply remain in the neutral semiconductor until it gives up its excess energy and recombines with a hole. A hole produced by such an electronic excitation may, if it is generated near the depletion layer edge, diffuse into the depletion layer and be swept by the field there to the surface, and thus contribute to photocurrent. The diffusion length for holes in n-type ionic materials however, is consistently extremely short; therefore this effect is neglected in the subsequent treatment.*

From the above discussion, it is apparent that the contribution to photocurrent due to light absorbed at a given distance into the crystal x is equal to the electronic charge times the number of photons absorbed at that depth:

---

*The assumption that hole diffusion contributes negligibly to photocurrent can be experimentally checked (although in the present work the experiment has not been attempted.) This statement is amplified in Appendix B.

$$\frac{dJ}{dx} = q\left[-\frac{d\Phi(x)}{dx}\right] \tag{15}$$

where $\Phi(x)$ is the photon flux per unit area at depth x in the crystal, and J is the photocurrent per unit area. Thus, the total photocurrent per unit area is

$$\begin{aligned} J &= q\int_0^w \left[-\frac{d\Phi(x)}{dx}\right] dx \\ &= q[\Phi(0) - \Phi(w)] \end{aligned} \tag{16}$$

where w is the depletion layer thickness.

For the case of a crystal of sufficient thickness that $\alpha d \gg 1$, the photon flux at x will contain no component due to reflection from the back of the sample, but only light transmitted from the front surface. $\Phi(0)$ is by definition the flux just inside the metal-semiconductor interface (after any losses due to absorption in the metal and reflection at the interface); thus, the photon flux in this case should follow the simple exponential law

$$\Phi(x) = \Phi(0)\, e^{-\alpha x} \tag{17}$$

Finally, equation (17) can be substituted into equation (16), giving the dependence of photocurrent on incident intensity $\Phi(0)$, depletion layer thickness w, and absorption coefficient α :

$$J = q\Phi(0)[1 - e^{-\alpha w}] \tag{18}$$

Thus, if $\Phi(0)$ and J can be measured as a function of wavelength,

and w determined, then $\alpha(\lambda)$ can be derived simply by the use of equation (18).

An interesting limiting case of this expression occurs if essentially all the incident light is absorbed within the depletion layer. In this case $e^{-\alpha w} \to 0$ and $J \simeq q\Phi(0)$. We may call this quantity the saturation photocurrent per unit area

$$J_o \equiv q\,\Phi(0) \tag{19}$$

and the ratio J/J_o is evidently the quantum efficiency Q of the Schottky barrier structure (considering only processes internal to the semiconductor.)

Using this definition of Q and solving equation (18) for α gives the form of this equation best suited to analysis of experimental data:

$$\alpha(\lambda) = -\frac{1}{w}\,\ell n[1 - Q(\lambda)] \tag{20}$$

Here w and $Q = J/J_o$ are to be experimentally determined, and α is the quantity sought.

D. Photocurrent Measurement: Experimental

The experimental sample used for this measurement was a plate of Ga_2O_3 cleaved, in the manner described in the Introduction, to a thickness of ~82μ. A semitransparent film of gold, covering a circular area of about 1 mm diameter, was evaporated through a mask onto one of the cleaved surfaces (hereafter referred to as the "front" surface of the sample) in a vacuum of ~10^{-6} torr. Subsequently, the other cleaved surface was entirely covered with vacuum-evaporated aluminum. This

aluminum layer formed an ohmic contact to the bulk of the sample, while the gold layer formed a Schottky barrier on the front of the sample.

The zero-bias small-signal capacitance of the Schottky barrier was measured; from this value (1896 pf), the gold dot diameter (1.127 mm), and the known[14] dielectric constant of Ga_2O_3 (10.2 ± 0.5), the Schottky barrier depletion layer thickness was calculated to be 475Å ± 5%.

The determination of α from photocurrent has the disadvantage of requiring two independent <u>absolute</u> measurements to be performed. (The transmission measurement, in contrast, involves measuring a ratio, with no absolute system calibration being required). Thus, errors in both sample photocurrent and incident intensity determinations appear linearly in Q, and correspondingly in α. (The sensitivity of α to errors in Q is explored in appendix C). The accuracy of the photocurrent measurement, which was accomplished using a PAR Model 122 lock-in amplifier together with a PAR Model 112 preamplifier, is estimated from manufacturer's specifications to be about ± 3%. The determination of $\Phi(0)$, the photon flux per unit area at the front surface of the semiconductor, presented the greatest experimental difficulty, and its estimated accuracy is no better than approximately ± 20%.

The first difficulty in measuring the incident flux was in obtaining a calibrated photosensor. In the present instance, this objective was pursued in two steps. First, a Reeder radiation thermopile with a quartz window was exposed to a commercial "black body" radiation source at 600°C, which was chopped at 50 Hz (the same frequency used in the photocurrent measurement). Using various aperture sizes in front of the black body and various distances between it and the thermopile

an average sensitivity was obtained. When corrected for the cutoff of transmission of the quartz window at about 4μm, the sensitivity of the thermopile was considered to be known to about ± 10%. (The greatest uncertainty in this calibration is due to the window transmission, which had to be calculated from published data and the measured thickness). Finally, an RCA type 935 vacuum photodiode (S-5 response) was calibrated against the Reeder thermopile, at wavelengths covering the range of interest, using the Gaertner monochromator as a source. This photodiode, because of its relatively great sensitivity and its stability, was used in the actual measurement of $\Phi(0)$. (The additional error introduced by its one-remove from the original irradiance standard is estimated, primarily from reproducibility checks, to be <2%).

The problem of obtaining an adequately calibrated photosensor having thus been solved, there remained the problem using it to determine $\Phi(0)$. As mentioned above, this quantity represents the light flux just <u>inside</u> the semiconductor. Thus, it is smaller than the flux externally incident on the sample to the extent of reflection from the surface of the metal layer, absorption in the metal, and reflection at the metal-semiconductor interface. These quantities cannot be calculated <u>a priori</u> from the bulk optical properties of the metal, since the optical properties of thin metallic films are known to vary drastically depending on film thickness and substrate.[15] Therefore $\Phi(0)$ must be inferred from light <u>transmitted</u> by the sample. The manner in which this transmitted light is related to the desired quantity $\Phi(0)$ is explained with the aid of fig. 10.

Fig. 10 shows the physical arrangement of sample beam, and a metal mask pierced by a hole slightly smaller than the gold dot, which was used in determining $\Phi(0)$. (Note that this determination was carried out <u>before</u>

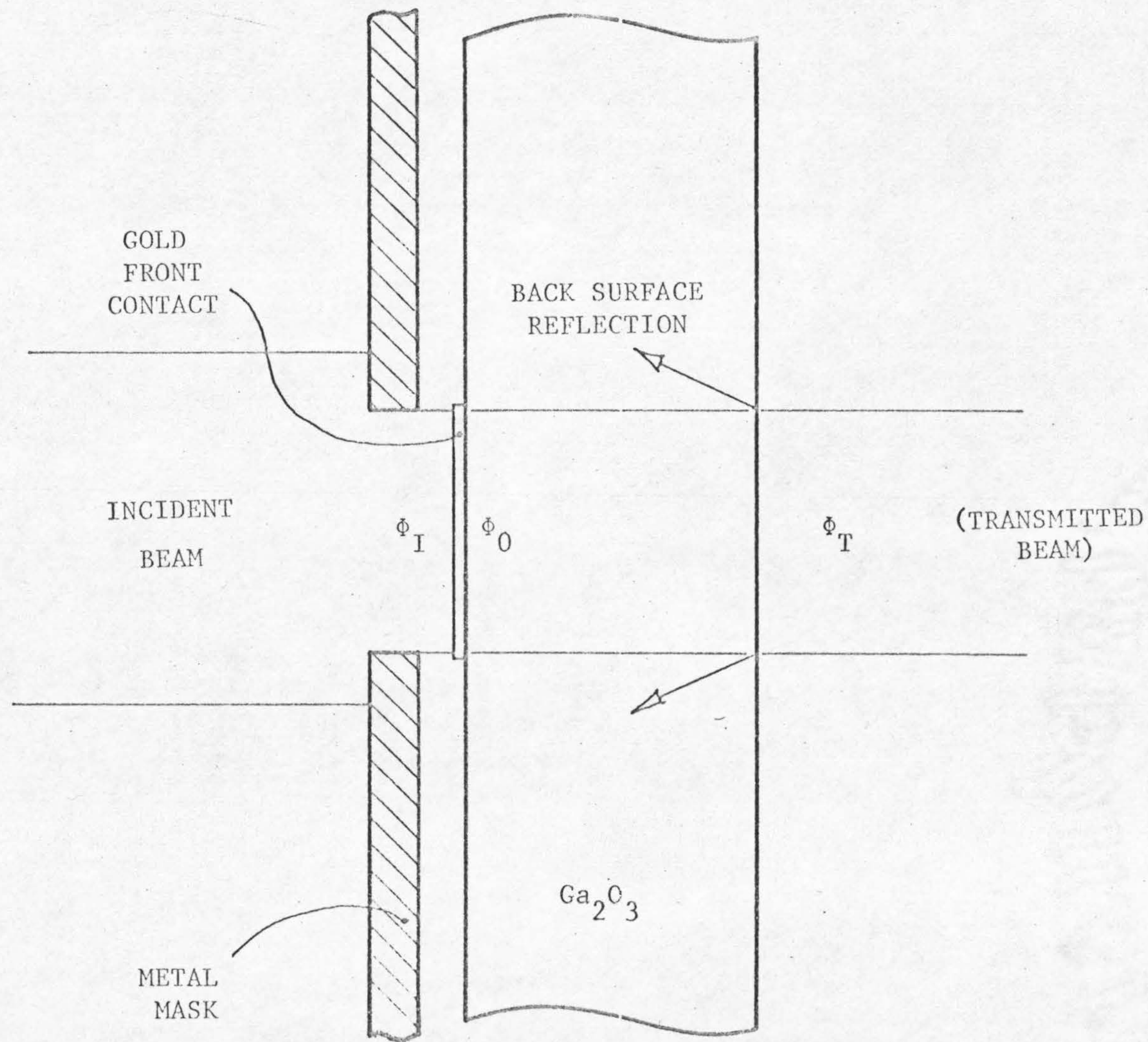

FIGURE 10. Schematic representation of sample and beam geometry in photocurrent measurement, showing various components of the incident beam.

the back of the sample was aluminized). A portion of the beam from the monochromator is passed by the metal mask; this portion, having a <u>total</u> photon flux* Φ_I, is the beam incident on the sample. Some fraction of this incident flux is transmitted to the semiconductor side of the metal-semiconductor interface; this transmitted fraction Φ_o, is the flux sought. Some fraction of ϕ_o, depending on absorption in the semiconductor, reaches the back surface; there, a further fraction is reflected back into the semiconductor (subsequent reflections are neglected) and the remainder emerges from the sample as the transmitted flux, Φ_T.

The transmitted flux, Φ_T, and the incident flux, Φ_I can be measured (the latter, with the sample removed). Their ratio is here defined as $f(\lambda)$,

$$f(\lambda) \equiv \frac{\Phi_T}{\Phi_I} \tag{21}$$

At a wavelength at which sample absorption is negligible, the transmitted flux is simply related to the desired Φ_o,

$$\Phi_T = (1-R)\ \Phi_o. \tag{22}$$

Thus, at such a wavelength, we have

$$\Phi_o = \frac{f(\lambda)\Phi_I}{(1-R)} \tag{23}$$

Unfortunately $f(\lambda)$ tends rapidly to zero as the wavelengths of interest are approached, since at these wavelengths the sample is strongly absorbing. (Φ_I can, of course, be measured at all relevant

---

*Since the flux per unit area is of value only in a uniform beam, quantities representing total flux (and total sample current) will be used hereafter. Thus, for example, Φ_o will be discussed instead of $\Phi(o)$.

wavelengths, and R can be calculated from the previously measured $n(\lambda)$ or its extrapolation). The procedure adopted in this work has been to extrapolate $f(\lambda)$ from the wavelength region in which it can be measured into the region of interest, in which it cannot be measured. This procedure seems justifiable, since the refractive index of Ga_2O_3 and the optical properties of Au (on which $f(\lambda)$ presumably depends) do not vary strongly or discontinuously with wavelengths in this region.

The experimental values of $f(\lambda)$, and the extrapolation initially made, are shown in fig. 11. When this extrapolated $f(\lambda)$, together with measurements of Φ_I and the total sample photocurrent I were used to calculate $Q(\lambda)$, values of Q greater than one were found at very short wavelengths ($\lambda < 0.25\mu m$) for light polarized perpendicular to the crystalline b-axis. Since the quantum efficiency for this structure cannot theoretically be greater than one, this result suggests that the calculated values of Φ_o are smaller than the actual flux. Whether this error was due to an erroneous extrapolation of $f(\lambda)$ or a calibration error in photocell sensitivity is unknown. However, since at these short wavelengths the calculated quantum efficiency was virtually independent of wavelength (that is, Q appeared to reach a limiting or saturation value) and this value was calculated to be slightly greater than one, it was assumed that the limiting value was actually the one normally expected of Q, that is Q = 1. This assumption yielded a further calibration point on the $f(\lambda)$ curve; for we can write

$$1 = Q \equiv \frac{I}{q\Phi_o} = \frac{I(1-R)}{Qf(\lambda)\Phi_I} \qquad (24)$$

and solve this equation for $f(\lambda)$. The resulting point is plotted on

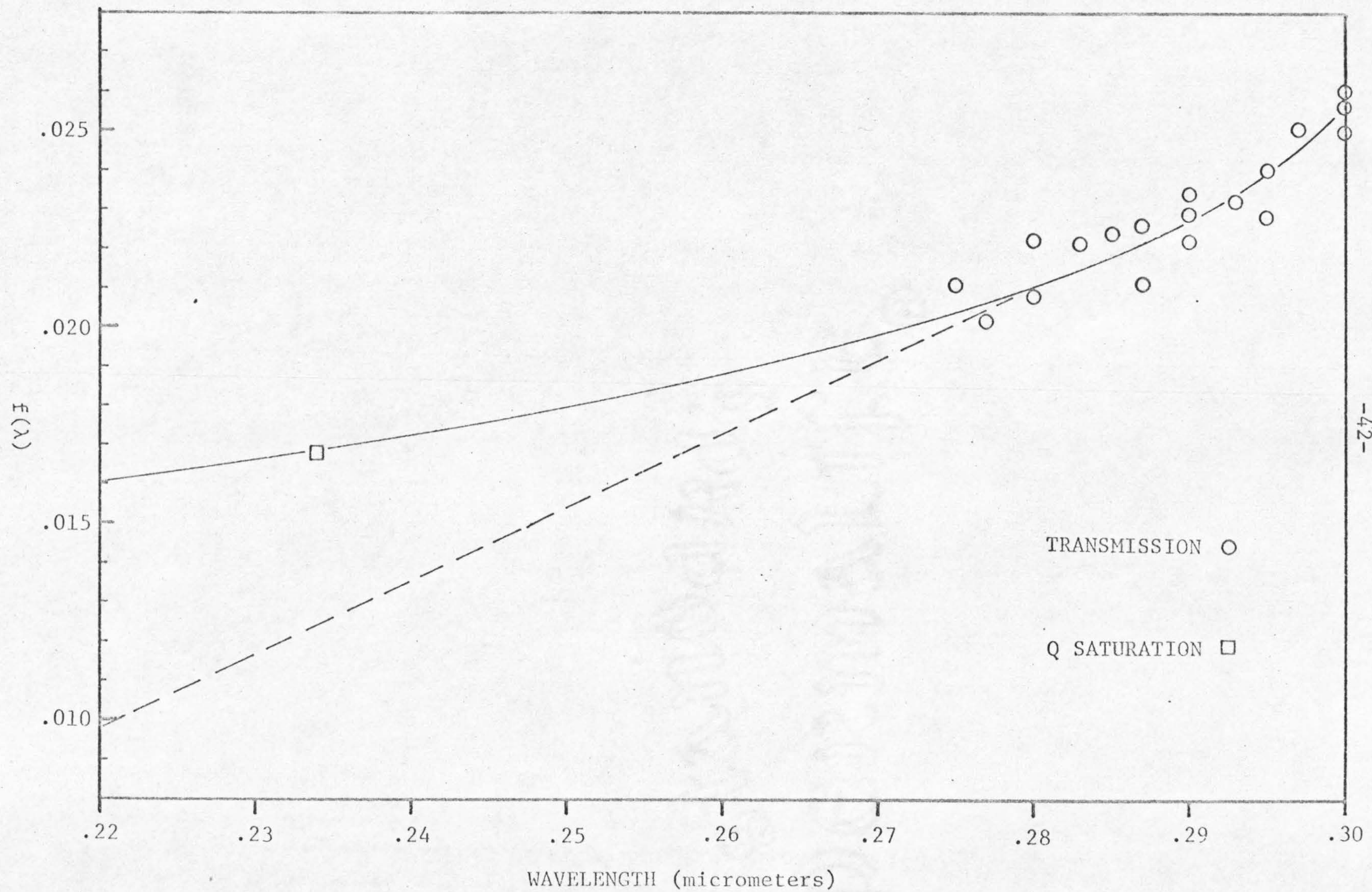

FIGURE 11. The factor f(λ) used in calculating effective incident intensity in the sample.

fig. 11, and a new "extrapolated" curve of $f(\lambda)$ made to pass through it. (As can be seen, the change was not large, amounting to about 30% at short wavelengths). This final curve should yield Φ_o to values accurate to ~ ± 3% (the photocurrent measurement accuracy) at the short-wavelength extreme, degrading more or less uniformly to the estimated accuracy of the photon-flux measurement (~ ± 15% at the long-wavelength extreme.)

The values of Q calculated using this final $f(\lambda)$ are shown in Fig. 12, for both polarizations. (The estimated accuracy of Q is the same as that of Φ_o, discussed above). From these points corresponding values of α can be calculated using equation (20). (The estimated accuracy of the calculated value of α is discussed in Appendix C). These values of α are plotted in fig. 13 (open circles). The filled circles are values of α calculated from transmission, i.e. the same data as that displayed in fig. 8; except that different samples are not distinguished in fig. 13. The agreement seen between α values calculated using the two methods is substantial, particularly in the case of the lower-energy edge, with polarization perpendicular to the b-axis. The discrepancy in the case of the other polarization has not been satisfactorily explained. Consideration of possible error sources suggests that the values determined from transmission should be trusted in preference to those from photocurrent.

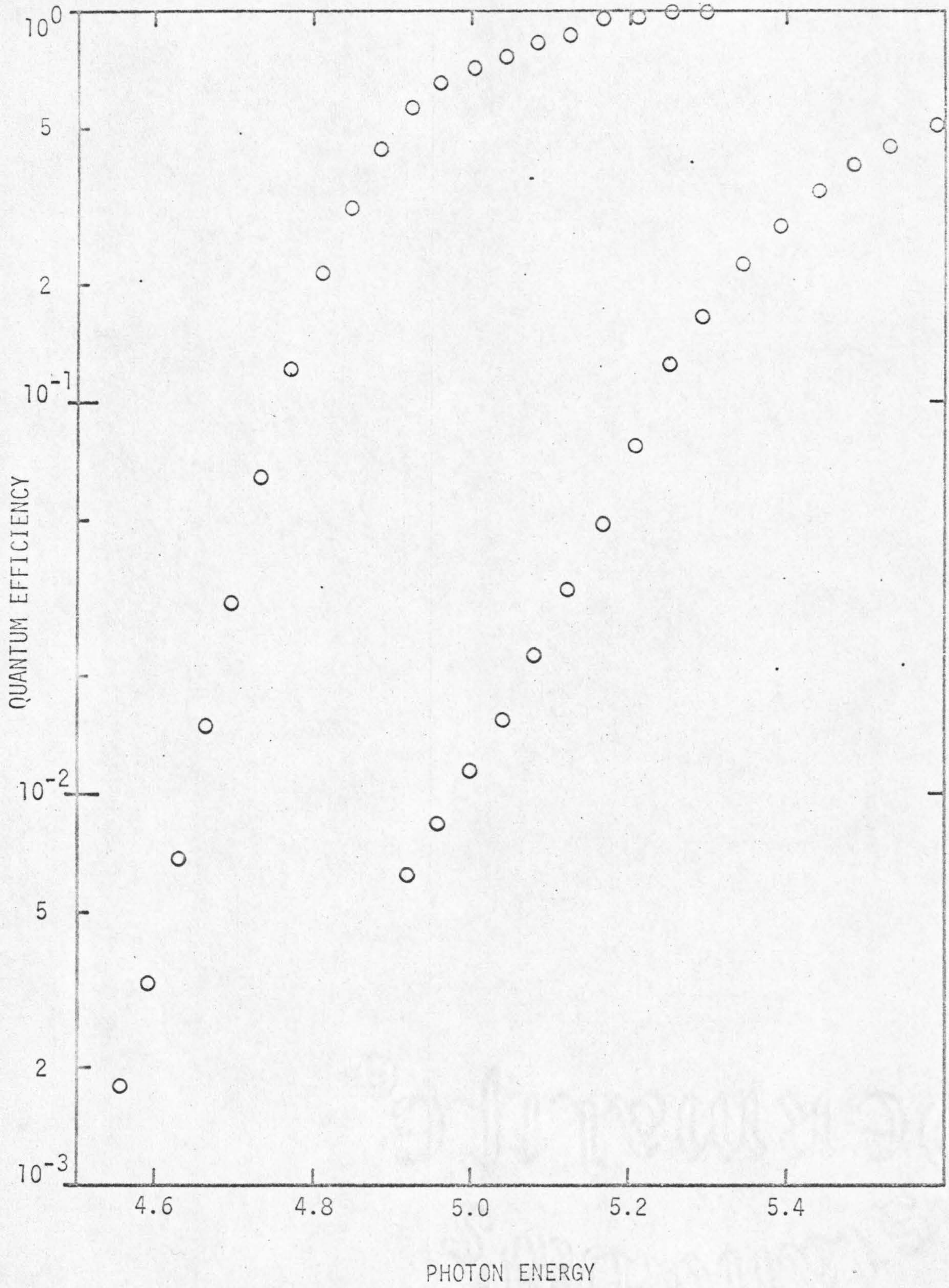

FIGURE 12. Measured Quantum Efficiency (see text) vs. photon energy.

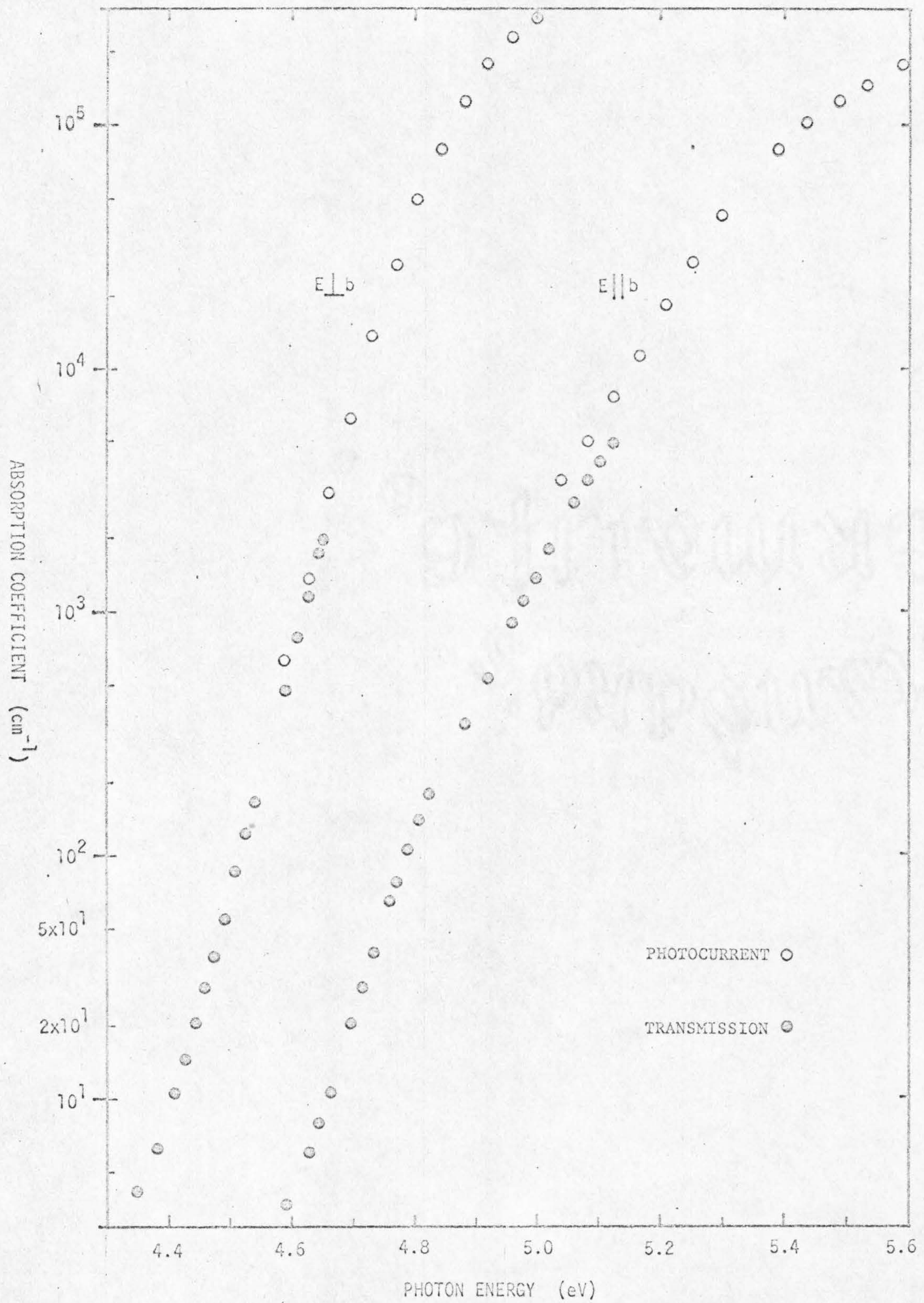

FIGURE 13. Absorption coefficient vs. photon energy for both incident polarizations and both methods of measurement.

IV. Conclusion

This thesis reports an experimental determination of the refractive index and optical absorption coefficient of β-Ga_2O_3. The values determined for these constants are presented as functions of wavelength in figures 5,6, and 13. The experimental techniques employed were developed for the particular set of difficulties and opportunities presented by the material properties of gallium oxide; however, since a number of other materials share some of these properties, it is expected that the techniques may prove useful to other investigators.

Because of the tendency of β -gallium oxide to cleave into thin plates with parallel faces, the conventional (prism) methods of refractive index determination are not usable with it, but another technique, exploiting interference due to multiple internal reflection within the plates, was successfully used to determine the refractive index over a wide range of wavelengths. This is the first application, known to the author, of this technique over an extensive wavelength range, particularly in the visible and ultraviolet spectral regions. The technique has been shown to possess the property, not previously reported, of revealing the existence of even a very slight birefringence in a spectacular manner, and allowing its quantitative measurement without the use of polarized light. A detailed analysis has been presented of this application of interference to refractive index determination; the technique should be of general utility in investigating the fairly large class of materials that exhibit a strong tendency to cleave into layers.

Two experimental approaches were used in the measurement of the absorption edge. For low values of α ($\alpha \lesssim 10^4$ cm^{-1}) the conventional technique of measuring transmission of thin samples was used. The application of this method for $\alpha > 10^4$ requires the use of samples of thickness of order 1μm which are extremely difficult to prepare and handle; for this reason, a new technique has been developed which effectively utilizes an absorbing layer less than 0.1μm thick. This technique makes use of the fact that, for the fundamental absorption edge of a semiconductor, each photon absorbed generates an electron-hole pair. By collecting the carrier pairs generated in the thin depletion region of a Schottky barrier, a photocurrent is obtained which can be related to the absorption occurring in the same thin region. Using this technique, the absorption coefficient measurement has been extended to $\alpha > 10^5$.

REFERENCES

1. M.R. Lorenz, et al., "Some Electrical Properties of the Semiconductor β-Ga_2O_3", J. Phys. Chem. Solids 28, p. 403 (1967).

2. S. Geller, "Crystal Structure of β-Ga_2O_3", J. Chem. Phys. 33, No. 3, p. 676 (1960).

3. H.H. Tippins, "Optical Absorption and Photoconductivity in the Band Edge of β-Ga_2O_3", Phys. Rev. 140, No. 1A, p. A316 (1965).

4. G. Blasse and A. Bril, "Some Observations on the Luminescence of β-Ga_2O_3", J. Phys. Chem. Solids 31, p. 707 (1970).

5. W.C. Herbert, et al., "Self-Activated Luminescence of β-Ga_2O_3", J. Electrochem. Soc. 116, No. 7, p. 1019 (1969).

6. C.A. Mead, "Metal-Semiconductor Surface Barriers", Solid-State Electronics 9, p. 1023 (1966).

7. S. Kurtin, T.C. McGill, and C.A. Mead, "Fundamental Transition in the Electronic Nature of Solids", Phys. Rev. Letters 22, No. 26, p. 1433 (1969).

8. A.B. Chase, "Growth of β-Ga_2O_3 by the Verneuil Technique", J. Am. Ceram. Soc. 47, No. 9, p. 470 (1964).

9. O.S. Heavens, Optical Properties of Thin Solid Films, Dover, New York, 1965, p. 55ff.

10. M.R. Tubbs, "Dispersion Studies of Ionic Crystals with Layer Structures", J. Phys. Chem. Solids, 27, p. 1667 (1966).

11. J.F. Nye, Physical Properties of Crystals. Oxford University Press, London, 1969, p. 235ff.

12. M. Born and E. Wolf, Principles of Optics, Pergamon Press, Oxford, 1970, p. 678 (footnote).

13. M. Born and E. Wolf, op. cit., pp. 678-9.

14. B. Hoeneisen, private communication.

15. O.S. Heavens, op. cit., p. 4.

16. B. D. Cullity, Elements of X-Ray Diffraction, Addison-Wesley, Reading, Massachusetts, 1959, p. 11.

17. B. D. Cullity, op. cit., Appendix.

18. International Union of Crystallography, International Tables for X-Ray Crystallography, V.III, Kynoch Press, Birmingham, England, 1962, p. 157 f.f.

Appendix

A. Details of Sample Thickness Calculation

As shown in part A of section I (eqn. (5c)) the raw data obtained from the channelled spectrum (fringe order, relative to some arbitrary "first" fringe, vs. wavelength) can be used to calculate the ratio of the thicknesses of two samples.

In practice, since the experimental data, especially for very thin, small-area samples, exhibit considerable scatter, one would like to include all data from a sample whose thickness is unknown in some calculational procedure which permits a meaningful average to be taken over them to determine a "best" value of sample thickness. Such a procedure is described below.

Rewriting eqn. (5c) as follows,

$$m_{II}(\lambda_a) = d_{II}\left[\frac{m_I(\lambda_a)}{d_I}\right] + m_{II}(\lambda_b) - m_I(\lambda_b)\left(\frac{d_{II}}{d_I}\right) \quad \text{(A1)}$$

it can be seen that a linear relationship exists between fringe order for a sample of unknown thickness (sample II) and the quantity $m_I(\lambda_a)/d_I$ which embodies data from a sample whose thickness is presumed known (sample I). Lumping the last two terms into a constant K (this step will be justified below) we can write the above equation simply as

$$m_{II}(\lambda) = d_{II} \cdot \left[\frac{m_I(\lambda)}{d_I}\right] + K \quad \text{(A2)}$$

in which the linear relationship is obvious.

Now, presuming that $m_I(\lambda)/d_I$ is available as a continuous function of sufficient accuracy, it becomes possible to include all data from sample II in a determination of d_{II}: for each data point (i.e.,

each fringe, specified by an order m_{II} and a wavelength λ at which the fringe occurs) m_{II} is plotted against $m_I(\lambda)/d_I$. The resulting set of plotted points is then fitted with the best straight line (either graphically, or numerically if desired) and the slope of that line,

$$d(m_{II})/d\left[\frac{m_I(\lambda)}{d_I}\right] \tag{A3}$$

is the desired thickness d_{II}. Thus all data points from sample II have been included in the determination, as desired, and the difficult problem of fitting an unknown function $m_{II}(\lambda)$ with a "smooth curve" has been reduced to the relatively simple one of finding the best straightline fit to a set of experimental data.

Two points in the above discussion require further explanation: the simplification involved in passing from eqn. (A1) to eqn. (A2); and the presumption that a continuous function $m_I(\lambda)/d_I$ which embodies the fringe data of the reference sample, can be obtained.

The first point can be justified by noting that the two terms which have been lumped as "K" are functions of a wavelength λ_b which is arbitrary, (i.e., eqn. (A1) is true for any particular value of λ_b) and which can therefore, in principle, be fixed at some definite value. Then, although the position of the $m_{II}(\lambda)$ vs $m_I(\lambda)/d_I$ curve depends on the value chosen, the slope of that curve, which is the number sought, does not. We can therefore assume that some λ_b was chosen, yielding the value K for the terms indicated, and then forget about K, since it has no effect on the further analysis of the data. (It may be mentioned here that any offset in fringe order disappears in the present analysis in a manner exactly analogous to the cancellation discussed in connection with eqn. (5c)).

In order to discuss the availability of a continuous function $m_I(\lambda)/d_I$, consider eqn. (8) rewritten as follows:

$$\frac{M(\lambda)}{d} = 2n(\lambda) \cdot \frac{1}{\lambda} - \frac{M_o}{d} \qquad . \qquad \text{(A4)}$$

It is apparent from this equation that if, for the sample which is to act as a thickness standard (d is presumed known), the particular set of relative fringe orders characterized by M_o are divided by the known thickness d and plotted vs $1/\lambda$, a curve will be obtained which differs from a straight line only in proportion to the dispersion of $n(\lambda)$. Except for λ very near the absorption edge, this is a very slight deviation indeed; hence, a graphical (or, if more accuracy is desired, a polynomial) fit to the "standard" data is entirely feasible. (Note that M_o here effectively appears only in the constant K in equation (A2) and the particular value chosen for producing the reference curve $M(\lambda)/d$ is therefore immaterial).

To summarize the above discussion: a method has been described of easily and accurately representing the fringe-vs-wavelength data of a thickness-reference sample as a continuous function, and a procedure given for combining all the available data from a sample of unknown thickness, using the continuous reference function, to obtain a value of unknown sample thickness representative of a meaningful average over these data.

B. Determination of Hole Diffusion Length

In the derivation of equation (18) the effects of holes diffusing into the depletion layer were ignored. If hole diffusion is in fact of

importance, equation (18) must be accordingly modified to the following form:

$$J = q\Phi(0) \left[1-e^{-\alpha(W+L)}\right] \tag{B1}$$

where L is the hole diffusion length in the neutral semiconductor.

If a reverse bias (that is, a voltage which increases the barrier height seen by majority carriers in the semiconductor) is applied to the Schottky barrier, the result will be a change in depletion layer thickness.[6] Since chopped light is used for exciting photocurrent, the leakage current which flows in the sample under reverse bias will not be confused with the photocurrent. As a result, the depletion layer thickness can be varied at a constant wavelength, resulting in a variation of photocurrent at constant α; if J is measured at two values of W we may write two simultaneous equations,

$$J_1 = q\Phi(0) \left[1-e^{-\alpha(W_1+L)}\right] \tag{B2a}$$

and

$$J_2 = q\Phi(0) \left[1-e^{-\alpha(W_2+L)}\right] \tag{B2b}$$

in which J_1, J_2, W_1, W_2, and $q\Phi(0)$ can be experimentally determined, and we desire to find the value of L. These equations may be simplified by writing Q for $J/q\Phi(0)$; then, taking logarithms of both sides and rearranging terms, we have:

$$\alpha(W_1+L) = - \quad (1-Q_1) \tag{B3a}$$

and

$$\alpha(W_2+L) = - \quad (1-Q_2) \tag{B3b}$$

Finally, solving for L yields

$$L = \left[\frac{\frac{\ln(1-Q_1)}{\ln(1-Q_2)} W_2 - W_1}{\frac{\ln(1-Q_1)}{\ln(1-Q_2)} - 1} \right]. \tag{B4}$$

Thus, in principle, it is possible to derive a value of L from a measurement of quantum efficiency at two values of reverse bias.

C. Sensitivity of Calculated α to Experimental Errors

From the form of eqn. (18) it can be seen that an error in the assumed value of W will appear linearly (to first order) in α.

As discussed in Section III part D, J_o is considered to be the most likely source of error in the present work. The effect of an error in this quantity can be seen by rewriting equation (20), expressing Q explicitly as J/J_o:

$$\alpha = \frac{1}{W} \ln\left(1 - \frac{J}{J_o}\right) \tag{C1}$$

Differentiating this equation with respect to J_o, we get

$$\frac{d\alpha}{dJ_o} = + \frac{1}{W} \frac{1}{\left(1 - \frac{J}{J_o}\right)} \frac{1}{J_o^2} \tag{C2}$$

Rearranging terms and dividing by equation (C1) yields:

$$\frac{d\alpha}{\alpha} = \frac{Q}{(1-Q)\ln(1-Q)} \frac{dJ_o}{J_o} \tag{C3}$$

where J/J_o has again been expressed as Q. This equation gives the fractional error in α resulting from a fractional error in J_o.

In the limit of $Q \ll 1$, this equation becomes simply

$$\frac{d\alpha}{\alpha} \simeq \frac{dJ_o}{J_o} \tag{C4}$$

In the opposite limit, $Q \to 1$,

$$\frac{d\alpha}{\alpha} \simeq \frac{1}{(1-Q)\ln(1-Q)} \frac{dJ_o}{J_o} \tag{C5}$$

which diverges as $Q \to 1$. At an intermediate point, $1-Q=e^{-1}$ ($\alpha W=1$), we have

$$\frac{d\alpha}{\alpha} \approx 1.7 \frac{dJ_o}{J_o} \tag{C6}$$

It is interesting to compare this sensitivity of α to error in J_o to the estimate of such error in the present experiment. J_o is considered known to within the accuracy of the beam intensity measurement ($\pm$ 15%) at the long-wavelength extreme of the measurement ($h\nu = 4.5$eV; $Q \sim 10^{-3}$). In the wavelength range where $f(\lambda)$ is extrapolated this error may be expected to increase slightly (to perhaps $\pm$ 20%) but as the $Q = 1$ calibration point is approached the error approaches zero. Thus, to some degree the sensitivity of α to error in J_o and the expected error in J_o are complementary. At $Q \sim 1$, however, (the high - $h\nu$ extreme of the measurement) the accuracy of α is certainly very dubious.

D. Correction to Thickness Determination

As explain on p. 14 of the text, the single thickness measurement required in the refractive index determination was obtained by the use of X-ray absorption. In the course of his examination of this thesis, Dr. C. A. Barnes suggested that there might be systematic errors (in addition to the statistical ones considered) which could degrade the accuracy of this measurement.

The value of X-ray absorption coefficient used to calculate thickness from the measured absorption was obtained by the normal procedure[16] of computing the weighted average, for Ga_2O_3, of the mass absorption coefficients of Ga and O. The density of the material is required: this was calculated from the unit cell volume, which is known to far more than sufficient accuracy from X-ray diffraction studies.[2] The values of μ/ρ for the two elements were taken from the tables in Cullity.[17]

The value of the linear absorption coefficient, μ, so obtained, while adequate for absorption corrections in X-ray diffraction work (for which the tables were intended) has several important sources of error. First, is the fact that the actual values of μ/ρ quoted in the table, while given to three significant figures, are not necessarily accurate to better than about 5%.[18] This uncertainty arises, first, because the actual value of μ/ρ is not easy to measure with any better accuracy, depending particularly on sample preparation and physical state; and second, because the values quoted in the tables do not even represent the specific measurements (on each element) available, but are derived from an

empirical smooth function of atomic number and wavelength which is best-fitted to all elements for which μ/ρ has been measured.[18]

Second, there are several factors which can subtract intensity from the incident x-ray beam (other than the photoelectric effect which is the major contributor to absorption) and which depend strongly on the exact chemical and crystalline state of the atoms involved, leading to errors in the simple weighted average value of μ/ρ. These factors include Compton scattering and scattering from plasmons in the conduction-electron gas. (These same factors, plus coherent scattering effects, are primarily responsible for the above-mentioned uncertainty in the measured values of μ/ρ.)

For these reasons, the statistical error in the thickness determination is trivially small compared to other uncertainties inherent in the absorption measurement. Therefore a new determination of sample thickness was undertaken.

The method adopted for measuring sample thickness consists of viewing the edge of the sample (perpendicular to the main cleavage) under an optical microscope, and comparing the sample thickness thus observed to a microscopic length standard viewed alternately in the same microscope.

In order for this method to be valid, the sample's main cleavage must be accurately perpendicular to the focal plane of the microscope. Considerable pains were taken to insure this condition in sample mounting; the deviation from perpendicularity is estimated to be less than 5°, which translates into a maximum error in sample

thickness of - 0.4%. An additional source of error is the difficulty of precisely defining the "edge" of the viewed sample surface. This difficulty is reflected in the reproducibility of thickness measurements in a given microscopic apparatus and with a given sample: the variation was ~ ± 0.3%.

The measurement was carried out on two samples (No. 1 and No. 5) under several different microscopes. Several variants of the "filar" eyepiece were used for comparing sample thickness with a length standard ("stage micrometer"). Based on manufacturers' claims of accuracy for the microscopic systems and stage micrometers, and reproducibility among the various systems, as well as the error sources described above, an overall accuracy of approximately ± 1% is estimated for this thickness determination.

The thickness values obtained for the two samples were:

No. 1: 36.1 ± .4

No. 5: 58.2 ± .6

As can be seen by comparison with the table on p. 13, the x-ray measurement was indeed in error by - 5.3%.

Because the quantity derived from the channeled spectrum is $n(\lambda) \cdot d$, the error in d appears inversely in the assigned values of $n(\lambda)$. Thus, Figs. 4, 5 and 6 should be corrected by a constant multiplicative factor of 0.947. The absolute accuracy of the resultant refractive index is entirely determined by the thickness measurement reported in this Appendix: it is ± 1%. (Note that the _relative_ accuracy of refractive index, for example the ratio of

n at one wavelength to n at another, is very much better: it is determined primarily by scatter in the channeled spectrum data, and is $< 0.1\%$.)

The correction to sample thickness affects the value assigned to absorption coefficient, α, (Figures 8 and 13), in two ways. At the low - α extreme ($\alpha \lesssim 5$) the correction to $n(\lambda)$ will significantly affect the calculated value of α (due to errors in calculated reflection); these points may therefore be significantly in error. At values of $\alpha > 100$, for which the sample thicknesses were determined by X-ray absorption, the thickness correction applies linearly to α. This correction, however, is invisible on the scale of Fig. 8 and 13.